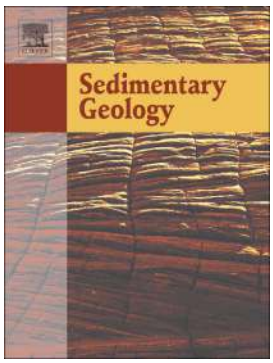

Sedimentary features influencing the occurrence and spatial variability of seismites (late Messinian, Gargano Promontory, southern Italy)

Michele Morsilli, Monica Giona Bucci, Elsa Gliozzi, Stefania Lisco, Massimo Moretti

PII: S0037-0738(20)30042-7

DOI: https://doi.org/10.1016/j.sedgeo.2020.105628

Reference: SEDGEO 105628

To appear in: *Sedimentary Geology*

Received date: 14 November 2019

Revised date: 27 February 2020

Accepted date: 28 February 2020

Please cite this article as: M. Morsilli, M.G. Bucci, E. Gliozzi, et al., Sedimentary features influencing the occurrence and spatial variability of seismites (late Messinian, Gargano Promontory, southern Italy), *Sedimentary Geology*(2020), https://doi.org/10.1016/j.sedgeo.2020.105628

Sedimentary features influencing the occurrence and spatial variability of seismites (late Messinian, Gargano Promontory, southern Italy)

Michele Morsilli [1], Monica Giona Bucci [2, 4], Elsa Gliozzi [3], Stefania Lisco [2], Massimo Moretti [2]

1 - Dipartimento di Fisica e Scienze della Terra - Università di Ferrara, Via G. Saragat, 1 – Ferrara, 44122, Italy.

(mrh@unife.it – https://orcid.org/0000-0001-6950-3659)

2 - Dipartimento di Scienze della Terra e Geoambientali, Università degli Studi di Bari "Aldo Moro", Campus Universitario, via E. Orabona 4, Bari, 70124, Italy

3 – Dipartimento di Scienze, Università Roma Tre, Largo San L. Murialdo 1, 00146 Roma, Italy

4 - Department of Chemical & Physical Sciences, University of Toronto Mississauga, 3359 Mississauga Rd Mississauga, ON, L5L 1C6, Canada

ABSTRACT

Seventeen layers characterized by soft-sediment deformation structures (SSDS) were identified within the "calcari di Fiumicello", an upper Messinian (Miocene) stratigraphic unit (30 m thick), cropping out in the northern sector of the Gargano Promontory (Apulia, southern Italy). Facies analysis was performed on the whole outcrop and detailed sedimentological investigations were carried out on the deformed beds, in order to interpret the deformation mechanism, the driving mechanism and the possible trigger agent. Deformed layers occur in some thin-bedded ooidal limestones, skeletal calcarenite, as well as in some pebble-size conglomerate, alternated with marls, deposited in a protected embayment or barrier-island-lagoon system, possibly characterized by high salinity, and tidal influx. SSDS can be classified as load- and slump/slide structures. The continuous exposures allow us to follow a single deformed layer along tens of meters, hence several types of lateral variations were observed that can be summarized as follows: (1) SSDS disappear within a few meters (with a decreasing pattern of their deformation or in an abrupt way); (2)

deformed layers laterally change in thickness and morphology; and (3) a single deformed bed can laterally correspond to two deformed beds. Most of the soft sediment deformation features were identified as liquefaction and/or fluidization features related to seismic shocks (seismites). Seismites are often used as an indicator of seismic events, especially along small outcrops, trench excavation and core analysis. This study highlights the value of the sedimentological analysis for paleoseismic investigations, with the aim of improving criteria for identifying seismites in the sedimentary record, and their suitability as marker of seismic events.

Keywords: Soft Sediment Deformations Structures (SSDS), Seismites, liquefaction, Gargano Promontory, Paleoseismicity

1. Introduction

The recognition and interpretation of soft-sediment deformation structures (SSDS) is the object of many papers (e.g.; Montenat et al., 1993; Moretti et al., 2016; Owen et al., 2011; Talwani and Amick, 1995). Seismically-induced layers with SSDS (seismites, *sensu* Seilacher, 1969) gained wide attention in sedimentological, structural and paleoseismic studies. Seismites have been recognised in: (a) sedimentary successions of different age (from Holocene Schneiderhan et al., 2005- to Archean); (b) all sedimentary environments from alluvial deposits (Allen and Banks, 1986; Pisarska-Jamroży et al., 2019) to pelagic successions (Haczewski, 1996); (c) all geodynamic settings, e.g., passive continental margins (Bezerra and Vita-Finzi, 2000), foreland (Moretti, 2000) and intracratonic areas (Tuttle et al., 2002), rift systems (Hilbert-Wolf and Roberts, 2015; Rodríguez-López et al., 2007), foreland basins (Hilbert-Wolf et al., 2009), intra-montane (Mohindra and Bagati, 1996) and strike-slip settings (Onofrio et al., 2009). Despite modelling of SSDS triggered by shaking (Moretti et al., 2011; Owen, 1996b), the analysis and identification of seismically-induced SSDS in the sedimentary record is still an open field of investigation, especially in terms of criteria for distinguishing these features by other types of SSDS. In the attempt to interpret SSDS as seismites, several criteria are

considered in the literature, and summarised as follows (Hilbert-Wolf et al., 2009; Jones and Omoto, 2000; Obermeier, 1996; Owen et al., 2011; Wheeler, 2002): (1) SSDS should be laterally continuous and interlayered by undeformed horizons, which allow the deformation to be clearly outlined; (2) SSDS are exposed with a vertical repetition; (3) ancient SSDS show morphological similarities with present-day earthquake-related liquefaction; (4) the sedimentary basin in which they occur is known to have been tectonically active; and (5) the distance from the earthquake epicentre influences the morphology or abundance of SSDS, due to the length of the liquefaction process. However, it is not always possible to apply these aforementioned criteria when specific geological conditions exist (Moretti and van Loon, 2014). For example, the lateral exposure of ancient seismically-induced SSDS could be limited by facies variation, and in particular by textural and water-saturation changes of the sediment bodies (Alfaro et al., 2010; Pisarska-Jamroży and Woźniak, 2019). Historical and present-day earthquakes confirm that the distribution of surface manifestation of liquefaction is strongly controlled by the geometry of water-saturated sandy layers and by their susceptibility to liquefaction process (Civico et al., 2015; Giona Bucci et al., 2018; Tuttle, 2001).

The vertical repetition of seismically-induced SSDS is used to assess the recurrence time of seismic shocks (Sims, 1975). However, often total liquefaction/fluidization of a sandy layer may result in lack or absence of appreciable deformation features, unless a driving force system takes place during liquefaction (Owen, 1987). In other words, the use of liquefaction features as estimator of earthquake recurrence time can be restricted by the chance that each seismic event has to leave a recognizable trace in the sedimentary record. The same layer can be affected by seismic liquefaction during multiple events; and, overprinting of SSDS can also be triggered by a single earthquake. Therefore, in the case of recurrence time calculated using ancient seismites, some authors prefer to employ the definition of “apparent” recurrence period of paleo-earthquakes (Ezquerro et al., 2016, 2015).

This contribution describes 17 individual SSDS layers in a 30 m-thick upper Messinian (late Miocene, from 7.2 to 5.3 Ma) succession called “calcari di Fiumicello” (Morsilli, 2005, 2016; Morsilli et al., 2017; Morsilli and

Moretti, 2009), and deposited in a semi-enclosed, low-energy, shallow marine/lagoonal setting (Morsilli, 2016). The sedimentary succession is characterized by sediments susceptible to liquefaction and detectable syn-sedimentary tectonics, in lateral continuity out along some rail trenches in the northern sector of the Gargano Promontory (Apulia, southern Italy). This makes the exposure ideal for investigating seismites. The site has relative absence of autogenic triggers ("internal to the system"; Owen and Moretti, 2011), and it presents occurrences of easily recognizable driving-force systems (essentially unstable density gradients and gravitational body forces)

The case study presented in this paper allows identification and interpretation of SSDS, characterized by lateral changes in the pattern of deformation, thickness, number of deformed beds, and their lateral persistence. The detailed sedimentary description will be used to identify variations in the pre-deformation system such as primary sedimentological lateral changes in geometry and texture of the layers affected by SSDS. The cases study will also be utilized to identify different deformation mechanisms/sediment behavior/driving force features acting during deformation. The environmental significance of seismites and their lateral changes within a specific sedimentary setting will be discussed in light of allogenic and autogenic trigger mechanisms. Results from this investigation will also provide insights about active tectonics and seismic events during the late Messinian in the northern part of the Gargano area.

2. Geological setting

The Apulia Region and part of the Adriatic Sea represent the foreland of both the NE-verging southern Apennine and the SW-verging Dinarides-Albanides thrust belts. The Gargano Promontory represents the northern sector of the Apulian foreland, showing moderate to strong deformed zones, and forms a broad gentle WNW-ESE oriented regional anticline (Brankman and Aydin, 2004). The Gargano Promontory (Fig. 1) is part of the Apulia Carbonate Platform, a major paleogeographic element of the southern margin of the Mesozoic Tethys Ocean (Bernoulli, 1972; Borgomano, 2000; Bosellini et al., 1999a) being one of the so-called

peri-Adriatic platforms (D'Argenio, 1976; Eberli et al., 1993). The backbone of the Gargano Promontory consists of thick (3000–3500 m) Jurassic and Cretaceous shallow-water carbonates (Bosellini et al., 1993a, b), which pass to margin and slope-to-basin deposits (Borgomano, 2000; Bosellini et al., 1999b; Masse and Luperto Sinni, 1989; Morsilli and Bosellini, 1997). Younger carbonate rocks unconformably overlie the Mesozoic units: Eocene base of slope resediments (Bosellini et al., 1999b; 1993b; Morsilli, 2016), Oligocene shallow-water carbonates (Casolari et al., 2000; Morsilli et al., 2017) and Miocene to Pliocene carbonate deposits in scattered sectors of the Gargano Promontory (Casolari et al., 2000; D'Alessandro et al., 1979 ; Moretti et al., 2011; Morsilli et al., 2017).

The upper Messinian "calcari di Fiumicello" informal stratigraphic unit was defined in the new geological map of the Italian Geological Survey at 1:50.000 scale (sheet n° 384 "Vico del Gargano" http://www.isprambiente.gov.it/Media/carg/384_VICO_DELGARGANO/Foglio.html (Morsilli et al., 2017). Figure 2 represents a synoptic version of this map. The best outcrops of this unit are exposed along the rail trenches in proximity of the villages of Cagnano Varano and Carpino, along the southeastern side of the Varano Lagoon (Figs. 1, 2). The "calcari di Fiumicello" unit is 30 m thick, and paraconformably overlays alluvial fan to fan delta conglomeratic deposits (Fig. 2). The "calcari di Fiumicello" is considered to be of late Messinian age (Morsilli et al., 2017), stratigraphically equivalent to the well-known Mediterranean Lago-Mare event (Cipollari et al., 1999; Cita et al., 1978 ; Clauzon et al., 2005; Cosentino et al., 2005; Orszagsperber, 2006; Ruggieri, 1967).

The Gargano Promontory has been interpreted as a Neogene contractional belt (Bertotti et al., 1999; Ciaranfi et al., 1988) with many thrust structures previously interpreted as normal faults. According to Bertotti et al. (2001), until the early Miocene, the Gargano was poorly deformed, but during the Langhian to Tortonian a tectonic phase started to deform existing and syndepositional units with gentle folds and thrusts. Between the late Miocene and early (?) Pliocene, NE-SW trending normal faults developed in the Gargano area, leading finally the uplift of the Promontory. Brankman and Aydin (2004) suggest that the uplifted Gargano area is a

push-up structure related to E-W striking, left-lateral strike-slip faults. Evidence of Plio-Pleistocene syn-sedimentary tectonic movement has been documented in the western part of the Gargano Promontory (Spalluto and Moretti, 2006). Post-Pliocene deformation consists of gentle NW-SE trending folds and strike-slip faults (Bertotti et al., 1999). The middle-Pleistocene-Holocene uplift results from the buckling of Apulian foreland due to the higher hinge rollback of the northern Adriatic lithosphere with respect to the southern one (Doglioni et al., 1994). The Gargano Promontory is intersected by several tectonic lineaments, including normal, reverse and strike-slip faults (Argnani et al., 2009; Bertotti et al., 1999; Billi et al., 2007; Borre et al., 2003; Brankman and Aydin, 2004; Chilovi et al., 2000; Fracassi et al., 2012; Funiciello et al., 1992; Milano et al., 2005; Tondi et al., 2005). The most prominent structural feature is the Mattinata fault (Fig. 1), a regional E–W shear zone that crosses the entire Gargano area, and extends offshore (Gondola Line, Fig. 1) for many tens of kilometers (Argnani et al., 2009; Brankman and Aydin, 2004; De Dominicis and Mazzoldi, 1989; Di Bucci et al., 2006; Funiciello et al., 1992; Ridente and Trincardi, 2006; Tondi et al., 2005). Quite controversial is the kinematics of this structure (see Argnani et al., 2009, for a review). It has been interpreted as right-lateral (Bosellini et al., 1993b; De Dominicis and Mazzoldi, 1989; Doglioni et al., 1994; Finetti et al., 1989; Guerricchio, 1986), left-lateral (Billi et al., 2007; Favali et al., 1993; Funiciello et al., 1992; Salvini et al., 1999), right- to left-lateral inverted (de Alteriis, 1995; Gambini and Tozzi, 1996) or a reverse fault (Ortolani and Pagliuca, 1989).

Other important fault zones with recent activity have been recognized in the north-western part of the Gargano Promontory (Fig. 1): South of the Apricena area (NW-SE oriented Apricena fault; Patacca and Scandone, 2004) and between Apricena and Poggio Imperiale (E-W oriented San Giovanni in Piano fault Spalluto and Moretti, 2006); active tectonic along strike-slip faults has been reported around the Tremiti Islands (Fig. 1) located northwestward of the Gargano Promontory (Bertotti et al., 1999; Favali et al., 1993; Funiciello et al., 1992; Ridente and Trincardi, 2006). The northern Gargano area is considered an important shear zone by all previous authors. In particular, Bertotti et al. (1999, 2001) show how late Miocene tectonic activity in this area was much stronger than during the subsequent tectonic phases. In this scenario, it is

reliable to infer that strong earthquakes, at least comparable to the historical 1627 AD earthquake of Imax= X MCS and Ma= 6.7 (Del Gaudio et al., 2007; Milano et al., 2005; Patacca and Scandone, 2004; Piccardi, 2005; Tondi et al., 2005), affected the northern Gargano area during the Late Miocene. Furthermore, a genetic relationship between the 1627 AD earthquake and the occurrence of some liquefaction features has been established by De Martini et al. (2003) in the coastal sector of the northern Gargano Promontory.

3. Methods

Standard sedimentological analyses were carried out along the stratigraphic succession and three detailed logs (Fig. 2) have been measured to interpret the main facies. More than eighty samples have been taken to describe the microfacies observing washed residue of disaggregated material and thin sections. Micro-palaentological analyses (sampling and processing) were carried out on thirteen samples (Figs. 2, 3) collected from the marly-clayey levels cropping out at Trench 1 (8 samples), Trench 2 (3 samples), and Trench 3 (2 samples). Layers with SSDS were carefully described in terms of both main deformational patterns and texture of the rocks involved in the deformation. The geometrical data of the layers with SSDS (length, thickness and orientation of specific elements) were measured along their complete lateral exposure; the relationships between these qualitative and quantitative features and the stratigraphy were analysed. Identification of the deformation mechanisms, driving forces and trigger agents, of SSDS was carried out according to the methods fostered by Owen et al. (2011), Owen and Moretti (2011) and Moretti et al. (Moretti et al., 2016). This method involves the use of a three-stage approach to identify triggers. The first phase consists of a facies assessment (to establish the exogenic or endogenic nature of the trigger); the second phase is centred in a trigger-by-trigger assessment (to identify the most likely trigger); the third phase implies a general criteria assessment (to discuss other criteria to supports the favoured trigger).

4. The “calcari di Fiumicello” deposits

The “calcari di Fiumicello” unit is made up of an alternation of well-bedded fine-grained carbonate deposits, with marly limestones, marls, calcarenites and rare calcirudites (Fig. 3). Three main lithofacies have been recognized. The first lithofacies is represented by limestones, with a grainstone to packstone texture mostly made up by superficial ooids (mainly dissolved and sometimes recrystallized), and less abundant intraclasts and lithoclasts, arranged in 10 to 120 cm thick beds. This lithofacies appear frequently cross-laminated with current and wave ripple, or cross-stratified bidirectional and sigmoidal laminae at dune scale as well as low angle planar cross-lamination. Grain size for these grainstones to packstones ranges from fine- to very coarse-grained calcarenites. The second lithofacies occurs in marly limestone and marls, white to light brown in colour, with a variable bed thickness from 2 to 50 cm, frequently with very thin, mm-scale lamination. The third lithofacies shows conglomerate layers that are visible in various intervals of the stratigraphic sections (Fig. 3) and have a thickness from 5 to 15 cm. They consist mainly of orthoconglomerate with clasts of 2 - 6 cm, derived from the Serravallian-Tortonian interval of the Pietra Leccese formation (Morsilli et al., 2017). Paraconglomerates with a sandy matrix are visible only at the top of Trench 1 (Fig. 3) where bed thickness increases up to 30 cm (Fig. 3). Elongated clasts reach the maximum size of about 10 cm. Potential exposure surfaces are associated with thick root traces, clearly visible in the marly intervals and also in some conglomerate beds of Trench 3 (Fig. 3). The detailed lithostratigraphy of the “calcari di Fiumicello” unit has been described along the rail trenches located close to the Cagnano Varano village (Fig. 2). The entire succession is gently deformed mainly by a post-Messinian tectonics, has a general tilting toward NE and shows some broad folds with axes NNW-SSE (Fig. 3). Some extensional faults (with a maximum displacement of few dm) are oriented N340°/65 and N150°/75. Some of these normal faults are syn-sedimentary while others seem to cut the entire “calcari di Fiumicello” unit. Nevertheless, the overall stratigraphy can be easily reconstructed and is shown in (Fig. 3) which illustrates also the vertical distribution of the units with SSDS. From the base to the top of the stratigraphic logs,

deformed layers were identified using alphabetical letters.

The lower portion of the “calcari di Fiumicello” succession is well exposed along the Trench 1 (about 8.5 m, Fig. 3). Here, ortho- and para-conglomerates (with abundant sandy matrix) alternate with coarse- and medium-grained oolitic calcarenites (grainstone/packstone) with traction features. Deformed units A and B occur in fine tomedium-grained calcarenites of this interval. Well-bedded laminated limestones (mudstone/wackestone) and marls occur in the middle part of the trench (between 4 and 6 m; Fig. 3). The succession visible in Trench 1 ends with parallel-laminated and very fine-grained calcarenites, calcisiltites and limestones (laminites with a mudstone/packstone texture). Here, in less than 2 m, three deformed units occur (C-E; Fig. 3).

The stratigraphic interval in Trench 2 (Fig. 3) is about 5.5 m thick and its lower portion is dominated by parallel laminated calcilutites and fine-grained calcarenites (with a high content of ostracods), with a general fining-upward trend, passing to laminites (mudstone/packstone alternation). The latter contain three thin deformed beds (deformed units F-H; Fig. 3). The upper stratigraphic interval of Trench 2 shows a clear coarsening-upward trend passing in a few meters to fine- medium- and coarse-grained calcarenites (packstone to grainstone) with traction features (mainly current ripples) and, in some places, narrow channelized erosional surfaces. Upward, crudely-bedded conglomerates (from ortho- to paraconglomerates) occur. The SSDS have the medium-grained calcarenites with ripple cross-lamination (deformed unit I) and the overlying coarse-grained calcarenites forming the very thick deformed units L and M.

The stratigraphic succession in Trench 3 is about 10.5 m thick and shows a lower portion (less than 2 m thick) with calcilutites and marls with rare thin and tabular microconglomerate beds. Erosional surfaces and root traces are widespread. Upward, the succession is characterized by medium-grained calcarenites (mainly ooidal grainstone) showing low-angle foresets, sigmoidal and tabular beds with localized deformed units (N and O, Fig. 3). The middle portion of Trench 3 (about 6 m thick) is represented by an alternation of decimetric intervals of parallel laminated (rare ripple cross-laminated) calcilutites, fine-grained calcarenites (mainly wackestone/packstone) and marls. Only the marls intervals contain two thin deformed units (P and Q, Fig. 3).

The upper part of the Trench 3 shows a very well laminated portion (about 1.5 m thick) made up of limestones (mudstone/wackestone). This interval with laminites ends with a thick deformed unit (R, Fig. 3). The succession of Trench 3 ends with ooidal coarse-grained calcarenites (grainstone) showing low-angle foresets.

4.1 *Micropalaentological data*

In the ”calcari di Fiumicello” unit, macrofossils are not present and microfossils in thin sections consist of rare remains of benthic and planktonic foraminifera. Bioturbation is always absent, with the exception of the intervals with evident root traces structures.

Only ostracods are very abundant: they are widespread in the middle and upper part of the “calcari di Fiumicello” (Trenches 2 and 3), while in the lower part (Trench 1) they are rare to very rare, except for some samples. The collected carapaces and loose valves are well preserved. Only on rare occasions, carapaces appear as incrusted and sometimes broken. The ostracod aggregation includes dominant *Cyprideis agrigentina* Decima, 1964, coupled with very few, badly preserved carapaces of *Sylvestra* sp., Candoninae indet., *Zalanyiella* sp., and *Loxoconcha muelleri* (Méhes, 1908). In those samples where *C. agrigentina* is abundant, the species is represented by adult females, males carapaces, valves, and a lot of loose juvenile valves, indicating *in situ* assemblages. In some samples, few valves bear 2-4 nodes), possibly characterizing a low salinity setting. Only occasionally, ostracods are observed along with few benthic foraminifers referable to genus *Ammonia*. The presence of *C. agrigentina*, *L. muelleri* and *Zalanyiella* sp. suggest the studied section is uppermost Messinian (late Miocene), in particular it belongs to the last phase (*lago-mare*) of the Messinian Salinity Crisis.

4.2 *Facies interpretation*

Based on lithologies, texture and sedimentary structures, five main facies have been recognized and interpreted as indicative of the following sub-environments: (1) very low energy lacustrine (mm thick

laminations) ; (2) shallow protected lagoon, sometimes colonized by mangrove (root traces); (3) small internal beaches composed of pebbles or sand size grains (foreshore – planar low angle laminations); (4) very small coarse grained fan delta (paraconglomerate); and (5) flood delta and/or small tidal bars (m-scale sigmoidal and bidirectional lamination).

Sedimentological and micropalaeontological data show that the calcari di Fiumicello unit was deposited in a lagoonal to protected semi-enclosed marine basin (maybe similar to the modern Varano Lagoon). In this small basin, minor sea-level changes and/or morphosedimentary variations (e.g., lagoon mouths dynamics) produced sudden facies migrations, mainly as result of water depth changes. Furthermore, this low-energy environment was locally influenced by the migration or lateral shift of tidal bars and flood delta deposits. Finally, the absence of epifauna and infauna (with the exception of ostracods) is a record of stressed salinity conditions or Eh=0 at the water-sediment interface during most of the basin evolution.

5. The soft-sediment deformation structures

5.1 *Morphology of the SSDS*

Log Trench 1 (*6 deformed units*)

The deformed unit A is about 25 cm thick and comprises homogenised fine- to medium-grained calcarenite (Fig. 4A). Narrow upward-directed laminae occur close to the bottom of the unit. Small-scale pillows (2-5 cm in height and 7-8 cm in width) of fine-grained calcarenite appear in the midst of this layer (between about 10-15 cm from the bottom of the unit), often showing a teardrop shape (*sensu* Owen and Moretti, 2008). Pillows are characterized by regular concentric laminae parallel to the outer edge. The deformed unit A extends for about 8 m laterally.

The deformed unit B (Fig. 4B) is nearly 20 cm thick and is characterised by calcilutites and fine-grained calcarenites. Deformation is represented by a regular alternation of large load-casts (4 cm in height and 10 cm

in width) and narrow flame structures that appear to cross the entire unit. These deformation structures pass laterally to undeformed primary parallel laminations in 1 or 2 m. Primary lamination is preserved both in the deformed and undeformed portion of this unit. The deformed unit B displays neither lateral change in thickness nor any appreciable lithological differences between deformed and undeformed portions, in both trench directions (SW and NE).

The deformed unit C (Fig. 4C) is nearly 40 cm thick, and about 50 m in total lateral extent. It is characterised by an alternation between medium-grained calcarenites and calcilutites. The southwestern portion (26.5 m of lateral extent) of the unit shows mainly load-structures, resulting in dm-scale ball-and-pillows floating in homogenised sediments. Locally, flame-structures, 20 cm in height, occur. There are variations in the morphology and thickness of the deformed intervals. North-eastwards, the deformed central portion of this unit passes laterally to an undeformed and parallel calcilutite laminated portion. At the same point, the upper and lower parts of unit C are exposed as distinct thinner deformed units (C1 - bottom sub-unit; C2 - top sub-unit). C1 and C2 sub-units show small-scale load-structures in coarse-grained calcarenites. Laterally, C1 and C2 slightly change their thickness and main deformation features. For example, C1, at first, decreases in thickness and is almost undeformed, but, in a few meters, it becomes thicker and deformed. Both C1 and C2 are observed laterally for 24 m.

The deformed unit D (Fig. 4D), 12-15 cm thick, consists of an alternation of fine-grained calcarenites and calcilutites. Deformation features are represented by large load structures (10 cm in height, 20 cm in width) with inner deformed laminations (parallel to the circular edge of the load structures). Pillows appear at different depths within this unit and contain whitish fine grained calcarenites or brownish medium-grained calcarenites. The primary lamination is not recognisable in the sediment surrounding the pillows. North-eastward, the deformation in the layer D gradually decreases until it disappears, within few meters.

The deformed unit E (Fig. 4E) is 3-7 cm thick and is represented by calcarenites and calcilutites. It shows an irregular and complex deformation of the primary laminations. Unit E shows a regular succession of folds, with

about 25 cm of wavelength. In more detail, whitish calcilutite laminae appear to be brecciated and thrusted, simulating slump-like features. Locally, they are broken and slightly rotated without a preferential orientation.

Log Trench 2 (*6 deformed units*)

This trench contains six deformed units (F-G-H-I-L-M). The F, G, H deformed units are a set of thin greyish calcarenite beds alternating with whitish calcilutite interlayers. Each deformed bed is always constrained by undeformed and well laminated fine-grained layers (Fig. 5A).

The deformed unit F is about 6 cm thick, and shows whitish fine-grained calcarenites. Deformation is highlighted by load casts (up to 3 cm in height, and 10 cm in width) with deformed primary lamination in their interior and homogenised sediment in the portions surrounding the load-structures. The deformation laterally fades away within 2 m, in both trench directions (SW and NE).

The deformed unit G is about 6-8 cm thick, and is made of well laminated medium and fine grained calcarenite. Deformation is represented by irregular load structures in which primary lamination is always preserved (Fig. 5A). This deformation gradually disappears within 2 m, in both directions (SW and NE).

The deformed unit H is about 12 cm thick, and it involves laminated medium- and fine-grained calcarenites. This unit shows narrow-spaced load structures (load casts and some balls distantiated apart of 15 cm). The core of these load structures does not often show evidence of primary laminations (Fig. 5). This deformed unit is no longer visible within 2 m from the observation point, in both trench directions (SW and NE).

The deformed unit I (Fig. 5B) affects a lenticular layer (8 cm thick), and it is characterized by medium-grained calcarenites. This unit is embedded in a series of undeformed calcarenitic layers with similar thickness and grain size. Deformation is represented by load structures very similar to the F, G, H deformed beds. This deformed unit disappears laterally (within 0.50 m in both trench directions NE and SW), as a result of its primary (lenticular) geometry.

The deformed unit L (Fig. 5C) has a variable thickness between 20 and 55 cm, and consists of coarse-grained

calcarenite. This unit is one of the thicker deformed layers of the studied succession. The whole deformed unit shows an irregular deformation of primary laminations (Fig. 5C). In the lower portion some load-structure features (pillows and upward directed flame structures) are well recognizable. Load structures are also observed in the upper portion, but they are locally masked by the presence of homogenized fine-grained sediments. The top of unit L is flat and represents the base of a laminated and undeformed cm-scale bed which separates this unit from the overlying deformed unit M (Fig. 5C-E).

The deformed unit M is 1.5-2.0 m thick and occurs in fine-grained calcarenite with rare coarse-grained calcarenitic and ruditic beds which are about 5 cmthick. Primary lamination is often folded or completely destroyed. The basal portion of this unit (20-30 cm thick) contains dm-scale tight folds (Fig. 5E, F): they are often asymmetrical (Fig. 5E) and a thickness variation between hinges and limbs is not observed. Upward, folds of the basal portion gradually pass to an interval of broken folds and breccias (for a total thickness of about 1 m); this interval gradually passes upward to undeformed beds. Measurements of axial planes of the folds that mainly involve the lowest portions of the unit M are very scattered showing a rough preferential orientation around W and SW dip directions (Fig. 5F). The deformed unit M extends for several tens of meters before fading away laterally and in both trench directions SW and NE.

Log Trench 3 (*5 deformed units*)

The stratigraphic succession in this trench contains five deformed units (N-O-P-Q-R). The deformed units N (Fig. 6A), O (Fig. 6B) and P (Fig. 6C) are closely associated with some medium- to coarse-grained calcarenites forming m scale foresets.

The deformed unit N (Fig. 6A) occurs just below coarse-grained calcarenites showing foresets at meter scale. It is 10-15 cm thick, made up of medium-grained calcarenites. Deformation is represented by 20 cm wide load-casts separated by narrow (few cm in length) upward-directed features. Primary laminations are deformed but always recognisable. This unit is characterized by a limited lateral extent (few cm on both sides, SW and NE),

because is cut by an upper irregular erosive surface.

The deformed unit O (Fig. 6B) occurs below some slight inclined calcarenite foreset beds and is 0.5 m thick. Unit O consists of whitish very fine grained calcarenites, and deformation is represented by localised large load cast (with a diameter up to 30 cm, preserving internal lamination), surrounded by homogenised/massive sediment. No lateral variation was observed for this unit.

The deformed unit P (Fig. 6C) is 6-8 cm thick, with medium to fine grained calcarenite, and occurs in sigmoidal beds with a variable inclination (from 12° to 20°, with a NW dip direction). Deformation is revealed as cm-scale slump-like morphologies passing laterally to broken laminae. Slump structures appear in the steeper part of the sigmoidal beds (locally, more than 20° in inclination, with a NW dip direction). No lateral variation was observed for this deformation unit.

The deformed unit Q (Fig. 6D) is 10-12 cm thick, and shows fine- and medium-grained (pink) calcarenites characterized by symmetrical and asymmetrical ripples. Deformation is represented by both distorted cross-lamination and load-structures with well-preserved internal lamination. Large load casts with 10 cm in width and narrow flame-structures (few cm in width) show always primary lamination. Unit Q passes laterally to undeformed alternations of fine- and medium-grained calcarenites with ripple cross-lamination. This deformed units extends in both trench directions, SW and NE, for several meters.

The deformed unit R is nearly 20-25 cm thick with medium- and fine-grained calcarenites showing sigmoidal lamination (Fig. 6E). Deformation is represented mainly by large load-casts, with 30 cm width. Internal lamination of load-structures is usually well preserved and is parallel to the edge of the load structure. Homogenised very fine-grained calcarenites and calcilutites surround the load-structures. Flame structures are recognisable between adjacent load-casts. At the inner edge of these large-scale load-casts, small-scale load-structures take place. Sudden lateral variations can be observed (Fig. 6E). Gradual lateral variations can be observed following the deformed unit R along many tens of meters. This unit shows always a clear distinction between a portion with load-structures (load-casts, ball-and-pillows and flame structures) with internal

lamination and a portion with homogenised and massive sediments Fig. 6E). These two different portions display different types of vertical distribution, which gradually alternate along the rail trenches. This deformed unit extends for several meters.

5.2 *Lateral variations of the SSDS*

Deformed units show extensive lateral variations given by changes in geometry, thickness, and deformation style. Three main types of lateral variations were observed and are listed as follows: (1) deformations extend for a very short length, up to 1 or 2 m (Type 1 – Fig. 7A); (2) laterally, deformation style and/or thickness gradually changes, and it can extends for several meters (longer than 2 m, and in some cases even over 10 m, Type 2 – Fig. 7B); and (3) a single deformed bed shows lateral bipartitions, and likewise the Type 2 variation, it can extends for several meters (Type 3 - Fig.7C).

Variations of Type 1 (Fig. 7A) affect the deformations identified as load structures and slump sheets with limited lateral extent (visible only for few m). Variation of Type 1 was observed, for example, in load structures below foresets prograding on a soft-substrate (unit O – Fig. 6B). Localised lateral variations were observed in slumped bodies slumped bodies within single high-angle foresets (unit P – Fig. 6C), irregular and laterally confined load casts (unit E – Fig. 4E), and deformed beds eroded by erosional surfaces (unit R – Fig. 6E).Deformed layers with this type of lateral variation often are no longer visible in few m (1 or 2 m).

In the variations of Type 2, deformation morphologies and/or thickness of the deformed units either laterally change along several meters (more than 2 m, and up to some tens of m), or they gradually decrease in thickness and complexity until fading away (Type 2 - Fig. 7B). Variations of Type 2 have been observed in the deformed units characterized by load structures, flames, in the calcarenitic layers A, B, C, D, F, G, H, I, L, Q and R. The most impressive and complex deformations were all observed in units characterized by at least 15-20 cm of thickness (e.g., deformed units C, I, Q and R). For instance, in the deformed unit R (Fig. 6E), load-

structures (load-casts, ball-and-pillows and flame structures) with internal lamination, and the homogenised parts can characterise different portions of the deformed bed and their relative occurrence can be observed along many ten of m. We have distinguished the following three types of deformed beds (Fig. 10B): (1) internal lamination and massive sediment pervasively involve the whole layer, (2) two portions with internal lamination and massive sediment occur within the same layer but not in phase, (3) laminated load-structures occur right at the top and at the bottom of the unit and are separated by the massive portion.

Variations of Type 3 is a unique example of SSDS that shows a very unusual lateral change. Unit C (Trench 1 – Fig. 3) shows some lateral variations of Type 2, but toward SE, it suffers a bipartition, and it turns into two sub-units (C1 and C2 Fig. 4C) separated by an undeformed set of fine-grained carbonate laminae (sub-unit Uc, in Fig 12). Laterally, the sub-unit Uc is completely involved in the deformation of the entire unit C, toward NW. Erosional surfaces and visible lateral lithologic changes in the involved beds were not observed (Fig. 4C).

5.3 *Evidence of synsedimentary tectonics*

Synsedimentary tectonics is recorded by many normal faults that involve the “calcari di Fiumicello” unit with displacement that typically decreases upwards. Often these faults induce some bed thickness changes between hanging wall and footwall portions. In Trench 2, some syn-sedimentary normal faults (dip direction – N30° and N200°) involve the deformed units L and M, causing an increase of their thickness in the hanging-wall portions (Fig. 5C). These small-scale faults seem to induce the formation of a slight topographic gradient towards the NE (Fig. 5C). A localised and small-scale graben-like structure (dip direction – N25° and N210°) shows unusual growth-fault features in the hanging-wall (Fig. 8). Furthermore, some small neptunian dykes (max 1.5 m in height and few cm in length) are present (Fig. 9). They are fissures that widen upwards and that are filled by soft-sediments coming from above. They are a record of synsedimentary extensional regimes as the above-mentioned faults.

Finally, small-scale faults (few cm of total displacement) affect many deformed units (Fig. 4C); they show an irregular vertical distribution, crossing the deformed unit C; these small-scale faults do not have a dominant dip direction and could not be associated with tectonics, being probably the effect of compaction during consolidation (Cartwright and Dewhurst, 1988) .

6. Discussion

6.1 *Interpretation of deformation mechanisms and driving force system for SSDS*

The mechanisms of deformation (*sensu* Owen, 1987) recorded by most SSDS in the "calcari di Fiumicello" formation are liquefaction and fluidization (viscous-fluid behaviour in load- and water-escape structures); some others show plastic and/or brittle behaviour (folds and breccia).

Load-structures are the most widespread SSDS in the analysed stratigraphic sections. They form in response to a driving force system (*sensu* Owen, 1987) related to an unstable density gradient (Rayleigh-Taylor instability). The gravitational re-adjustment starts only after a drastic reduction in shear strength of the involved sediments (Anketell et al., 1970). As a result of liquefaction, the interface between the two layers starts deforming, and then the two units with unstable densities gradient produce various kinds of load structures. Selective fluidization induced by the "re-settlement" of particles at the end of the liquefaction event (Allen, 1982; Owen, 1987) can also form some water-escape structures between adjacent load-structures (Moretti et al., 1999). In the load structures analysed here, the initial system is given by the overlying coarse-grained on fine-grained sediments. However, for some layers, the difference in bulk density is not obvious at the outcrop scale: in these cases, we have also investigated the reversed density gradient at the microscale (Fig. 10).Variations in deformation style observed in the load structures could be attributed to different parameters. The dynamic viscosity is the most important of these parameters, and differences in this quantity in two superposed units (Anketell et al., 1970) is responsible for the general sinusoidal morphology of the interface (with narrow or large antiformal and synformal features). The actual bulk density gradient and the

duration of the liquefaction state (Owen, 2003) is also a responsible factor that can induce slight deformations at the interface (load-casts – with lower density gradients and/or sudden end of the liquefaction/fluidization state), or the formation of ball-and-pillow structures (in high density gradient systems and/or for a long duration of the deformable state). Folds and slump-like features (deformed layers E, M and P) do not reveal associations with liquefaction and/or fluidization features at the outcrop scale. Therefore, we can infer that each individual plastic/brittle deformation characterizing the deformed layers E, M and P, occurred with lateral stresses acting as driving force system (gravitational body force of Owen, 1987), in conditions of reduced shear strength. Plastic and brittle deformations result in soft sediment that are generally associated with a slope, and the driving force system is related with lateral stresses (gravitational body force of Owen, 1987).

A slope surface was observed in the field as a morphological element for deformed layer P, where a foreset (more than 12° in dip) exposes irregular folds and thrust-like features and brecciation. Deformed layer E shows analogies with the morphological features observed in deformed layer P, but it involves only a set of sub-horizontal laminae (few cm thick). No obvious preferential orientation of the fold and axial planes has been observed.

The complex deformed layer M overlies on a sub-horizontal surface (corresponding to the top of deformed layer L), and in this case the presence of a slope can be inferred by measuring the axial planes of slump folds that occur mainly in the lower and middle portions of this deformed unit. W-SW dip directions are widespread, but data dispersion is generally high (see Fig. 5F). These results could be related with the presence of both non-cylindrical folds (in layer-parallel or -normal shearing conditions, Alsop and Marco, 2011) and/or slight and irregular slope gradients (Mastrogiacomo et al., 2012; Spalluto et al., 2007). Normal synsedimentary faults form small-scale horst and graben structures within unit M. These structural features probably contribute in creating a scattered low gradient slope system and a partial agreement between fault plane orientations and the shortening in the slumped unit M. Finally, the broken folds and breccia shows haphazard directions and records the brittle behaviour of some passively translated portions of the unit M during lateral movement.

6.2 *Interpretation of lateral variations in the deformed units*

Some authors have previously identified a lateral variability in beds with SSDS, but their studies are based at a basin scale analysis (e.g., Rodriguez-Lopez et al., 2007; Alfaro et al., 2010). In these studies, deformed layers were correlated over large distances (several km) and across different paleogeographical and paleoenvironmental settings. Furthermore, Gibert et al. (2011) interpret the occurrence of many superposed deformed beds passing laterally to a single deformed layer as result of liquefaction in a multilayered system with lateral permeability changes.

Data collected in the "calcari di Fiumicello" show the occurrence of seventeen units with SSDS, mostly characterized by extensive lateral variations given by changes in number, geometry, thickness, and deformation style. These lateral variations have been summarised in three main types that can be interpreted taking advantage of the direct observation of gradual and/or abrupt changes along continuous railway trenches.

The occurrence of Type 1 lateral variations (Fig. 7A) is related with the limited extent of the mechanisms that originate the SSDS. The localised load structures of the unit O form as result of the localised liquefaction features imposed by the prograding foreset on a soft substrate (Fig. 6B). Slumped bodies occurring within high-angle foresets (unit P - Fig. 6C) result from gravitational body forces acting on a limited amount of soft-sediment. Liquefaction in presence of unequal loading are responsible for the formation of localised load-casts of the unit E (Fig. 4E). Obviously, deformed layers can suddenly cease to be visible also for the presence of irregular erosional surfaces (as narrow channelized surfaces - unit R – Fig. 6E).

Lateral variations of Type 2 (Fig. 7B) connotates gradual changes in the morphology and/or thickness of SSDS. The occurrence of these lateral variations can potentially be associated with the primary sedimentologic

features of those units affected by SSDS, such as grain size and thickness of the layers affected by liquefaction/fluidization. Also, carbonate sediments can experience different degrees of early diagenesis (Bathurst, 1983). The lateral variations in the deformation style can be ascribed also to the additional presence of large-scale sedimentary structures characterising the pre-deformational system (Owen and Moretti, 2011). For example, the foresets or sigmoidal beds could be an additional heterogeneity given by the asymmetrical alternation of calcarenite and calcisiltite laminae. A lateral slight variation in the grain-size is visible in the sigmoidal beds but can only be supposed in the deformed ones since the primary lamination and the original textural features have been completely obliterated by the action of liquefaction and fluidization processes. The co-occurrence of a certain array of sedimentary structures (e.g., foresets) contributes in determining also the partitioning of liquefaction and fluidization features within the same unit, and thus the variety of SSDS morphologies observed in a single deformed layer.

Lateral variations of Type 3 (Fig. 7C) characterises deformed unit C which is characterised by a bifurcation toward the SE forming two sub-units (C1 and C2) separated by an undeformed set of fine-grained laminae (Uc). We interpret this atypical bipartition as the result of the thickening of the fine-grained sub-unit inducing a lateral variation of texture and permeability. . Here, the sub-unit Uc prevents the liquefaction of the whole set of strata (C=C1+Uc+C2) acting as a confining layer for the two sub-units C1 and C2, which still show evidence of deformation induced by liquidization (Scenario 1 in Fig. 11). Another possible explanations for this unusual lateral variation would infer the occurrence of an irregular erosional surface within the sediment that is not obvious in the field. However, this could lead to a very complicated scenario related to more sedimentary and erosional phases occurring in a relatively short time frame, and interrupted by two (Scenario 2 in Fig. 11) or three deformation events (Scenario 3 in Fig. 11).

The solution suggested in this paper (Scenario 1) has been qualitatively modelled using a simple analogical procedure (Supplementary material) reproducing a multilayered unstable density gradient system with lateral variations of permeability.

6.3 *Interpretation of trigger agents*

Liquefaction can be triggered by several natural processes. These are overloading or unequal loading, wave action, tidal action, sudden changes in groundwater table and earthquakes (Moretti et al., 2016). Discussions about this topic can be found in review papers such as Obermeier (1996), Owen et al. (2011) and Owen and Moretti (2011). As a consequence, similar morphological features will result from liquefaction triggered by different active natural agents responsible for liquefaction and/or fluidization (Dżułyński and Walton, 1965). This condition can represent a major issue when interpreting the trigger mechanism of SSDS. Therefore, facies analysis and a detailed description of the deformed layers aid in narrowing down the natural agent (or trigger mechanisms) causing liquefaction. According to Leeder (1987) and Owen and Moretti (2008), trigger mechanisms can be autogenic (related to depositional and/or erosive processes inside the sedimentary basin) or allogenic (such as seismic shocks or tsunamis). Prior to interpretation as a SSDS as induced by an allogenic process, a detailed discussion on the possible autogenic mechanisms is needed. In this study we used the procedure for determining the trigger mechanism of soft-sediment deformation proposed by Owen et al. (2011), that takes into account all possible triggers compatible with the sedimentary environments investigated at the site.

Overloading-related liquefaction and fluidization are driven by high rates of deposition (Lowe, 1975). Rapid deposition of a sandy bed may induce instantaneous increase in interstitial pore water pressure within the underlying bed. Quantitative estimations on the triggering effect of overloading are given in Moretti et al. (1999). Overloading and probably unequal loading can induce the deformation observed in the load-structures of deformed beds N and O (Trench 3). The latter occurs just underneath the foresets characterized by coarse-grained bodies: they represent the result of localised liquefaction effects of the soft substrate on which the

foresets rapidly prograde, inducing localized liquefaction effects. A very similar effect is described along the lee sides of prograding dunes in tidally-dominated deposits (Chiarella et al., 2016). No other evidence of overloading or unequal loading is documented.

Wave-induced liquefaction can result from the impulsive impact of breaking waves in proximal marine environments, but the cyclic effect of storm waves is generally considered more efficient in inducing liquefaction of unconsolidated sands (Henkel, 1970). The cyclic effect of storm waves is able to induce liquefaction at a considerable depth below the water-sediment interface (Molina et al., 1998) and it acts at the lower shoreface and offshore transition. The action of breaking waves on proximal beach environments, and storm-wave effects in deeper/distal deposits, is not likely here since the "calcari di Fiumicello" formation was deposited in semi-enclosed/lagoonal setting, in a generally low energy environment. Furthermore, despite some symmetrical ripples in coarse-grained pack-grainstones and very fine-grained calcarenites, the sedimentological features associated with the influence of storm waves are absent. Greb and Archer (2007) found evidence of soft-sediment deformation (from a few centimetres up to 17 cm of thickness) associated with the tidal action in modern estuarine sands in south-eastern Alaska. This type of SSDS is induced by macrotidal regimes characterized by 9-10 m of tidal range, and coupled with high-energy tidal bores (1.8 m in height, travelling at 16 km/h). During the Messinian, a microtidal regime can be inferred since the paleogeographic setting of the Mediterranean Sea did not change throughout the late Miocene (Roveri et al., 2014). As a consequence, at our study site the action of important tide as trigger mechanism is excluded because the microtidal influence would not be able to cause liquefaction and/or fluidization.

Other triggering mechanisms responsible for liquefaction and fluidization are less common, yet they own a preservation potential. Sand boils, or boiling springs (Guhman and Pederson, 1992; Holzer and Clark, 1993) are fed by discharge conduits of artesian ground water which may fossilize as large vertical cylinders of fluidized sand (Deynoux et al., 1990; Dionne, 1973). No evidences of localised upward directed flows have been

observed in the outcrop analysed for this study. Carbonate successions can be subject to large deformation related to the action of synsedimentary karstic processes (Moretti et al., 2011; Robledo and Pomar, 2000). This process commonly induces narrow downward collapses and sinkhole features that were not observed in the investigated succession.

Seismic shocks are the only other reliable trigger mechanisms for most of SSDS in the "calcari di Fiumicello unit (except for the deformed units E, N and O with autogenic origins). An extensive literature refers to palaeoseismic studies in Holocene sediments deposited in many sedimentary environments based on the analysis of liquefaction and fluidization structures corresponding to well-known historical, and instrumentally-recorded seismic events (e.g., Galli, 2000; Quigley et al., 2016; Tuttle et al., 2019; 2017; Villamor et al., 2016). Many authors report a genetic relationship between seismic shaking and SSDS (dykes, load-structures, deformed laminations, etc.) in field-based investigations of ancient deposits (*see* Moretti and van Loon, 2014, and references therein) and analogic modelling tests in laboratory (Kuenen, 1958; Moretti et al., 1999; Owen, 1996a).

Careful consideration is required for assessing the genetic interpretation of irregular folds and slump-like structures since no evidence of liquefaction and/or fluidization features was documented during the field campaign. The origin is clearly autogenic (peculiar to the system analysed) for slump-like structures observed in the deformed layer P (Fig. 4, Trench 3). Centimetric slump structures occur at the bottom of the lee-side of the foresets identified in Trench 3. Slump structures result from localised slide accumulation on the steeper side of the foresets during rapid progradation (Fig. 6C). An autogenic trigger was identified also for the deformed layer E (Trench 1, Fig. 4). This layer has got thin and localized slump-like laminae could be ascribed to minor perturbation processes at the water/sediment interface (like weak current shear stresses)

Dm-scale slump structures observed in the deformed unit M (Trench 2, Fig. 5E, 5F) occur on a sub-horizontal and undeformed (flat) surface (Fig. 5CE). Autogenic processes such as storm wave action, overloading, sudden changes in groundwater, tidal hydrodynamic processes can be all excluded on the basis of the same

assumptions illustrated above for load-structures. The slump body is characterized by about 50 cm of carbonate sediments in a lateral movement on a nearly flat surface (lagoonal floor). We interpret this unit as seismically-induced, inferring that only a sudden and drastic decrease in shear strength can result in the documented deformed features (shear folds at the base of the unit, and breccia formation in the whole body of the slump) on sub-horizontal surface. Other evidence is that the direction of shortening in the slump body (*see* the rose diagram of Fig. 5F) is roughly consistent with the orientation of main synsedimentary faults (Figs. 5C, 8). Likewise, the occurrence of slumps in modern (Field et al., 1982) and ancient tidal flat and shallow-sea environments (Bhattacharya and Bandyopadhyay, 1998; Rossetti and Santos Jr., 2003; Spalluto et al., 2007) is interpreted in terms of paleoseismicity.

6.4 *Inferring reliable paleoseismic parameters from seismically-induced SSDS*

The seismites recognized in this study seem to occur in ideal general conditions (sediments are susceptible to liquefaction, driving force systems acting during the deformation, absence of predominant erosive or sedimentary processes, vertical and lateral occurrence of deformed beds, moderate- to high-magnitude seismic area, etc.). Hence, the seismically-induced SSDS of the "calcari di Fiumicello" deposits can have a paleoseismic relevance which is worth to be discussed.

As shown in the field, the counting of SSDS can change laterally leading to either overestimation or underestimation of the recurrence time of the paleoseismic events. For example, each deformed bed can split in two. The field data represent a limitation the active tectonics analyses, especially if paleoseismic investigations are mainly based on the study of a single stratigraphic section and/or short paleoseismic trenches and well-logs. Nevertheless, the recurrence time of seismic events in this area can be roughly calculated by taking into account only the reliable seismically-induced SSDS (twelve). A sedimentation rate of about 1-2 mm/y was supposed, assuming data coming from a Holocene succession deposited in similar depositional settings (lagoonal to semi-enclosed marine basin), and located in analogous microtidal regime (e.g. Mar Piccolo basin, Southern Italy; Valenzano et al., 2018). As a consequence, the time of paleo-earthquake

event occurrence would be of few thousand years (2500-5000 years), given the number of seismically induced deformed layers (twelve) in the 30 m thick sedimentary succession. This result can slightly vary as a consequence of changes in sedimentation rate, as observed in the portions with coarse-grained sedimentary deposits of sigmoids or foreset, where some overloading effects have been detected. Nevertheless, this conclusion is not unreliable in terms of a timeframe, but it represents the "*apparent recurrence time*" of earthquakes with M>5 (*sensu* Ezquerro et al., 2015, 2016) in this area.

Secondly, the thickness and dominant morphologies of the deformed layers are strongly influenced by primary sedimentological features, in particular by structural (bedding and lamination) and textural features (grain-size, density of sediments, relative density of the sedimentary framework, etc.) of the involved layers, but also by their environmental setting: the position of the water table, liquefaction duration, and presence of a driving force system active during liquefaction. As a consequence, attempts to correlate thickness and/or the morphologies of seismites to a specific magnitude of paleo-earthquakes (as suggested in Berra and Felletti, 2011; Rodriguez Pascua et al., 2000) can prove challenging, and thus it is hardly limited by primary sedimentological conditions and environmental settings.

Many studies have aimed to reduce uncertainties of magnitude estimates of paleo-earthquakes from paleoliquefaction features by performing regional calibration of the magnitude-distance relation (Obermeier et al., 2002; Olson et al., 2005a; 2005b). Advances in this field of research were also tested by Green (2013) against the site specific geotechnical method (Idriss and Boulanger, 2006; Youd, 2001), using the 2010-2011 Canterbury Earthquake Sequence as a study case. Green's (2013) research assessed the back-calculated earthquake magnitude in two scenarios: known and unknown earthquake source locations. This investigation showed that the use of liquefaction surface effects triggered by events such as the Mw 7.2 2010 Darfield earthquake, (Basher et al., 2011; Hornblow et al., 2014; Quigley et al., 2012; van Bellegooy et al., 2014; Van Dissen et al., 2011) does not result in very accurate location of the earthquake epicentre. During the Darfield event areas that were far from the earthquake epicentre, but located in highly susceptible settings (Bastin et

al., 2016; Brackley et al., 2012) resulted as more liquefaction than areas close by. Therefore, it is valuable to take into account local conditions of liquefaction susceptibility for a better understanding of paleo-earthquake source.

Finally, comparing the occurrence of seismically-induced SSDS and the vertical distribution of main facies (Fig. 3), it seems that ideal conditions for the occurrence of liquefaction and fluidization processes are associated with lagoonal facies, obviously as result of widespread alternations of silt (potential permeability barriers) and sand (high susceptibility to liquefaction). These results are consistent with recent reports of liquefaction surface effects (EMERGEO, 2013; Tuttle et al., 2017; Villamor et al., 2016) and their association with specific alluvial geomorphic features as the point bar deposits and paleo meanders (Tuttle and Barstow, 1996; Giona Bucci et al., 2018).

7. Conclusions

Seventeen SSDS layers were identified in the Calcari di Fiumicello unit, and twelve of these are inferred to be seismites. The recognition of seismites at this site suggests that the Gargano Promontory was affected by strong (Mw > 5.0) and recurrent earthquakes at the end of the Miocene. The co-occurrence of (i) syn-sedimentary faults within the analysed outcrops, (ii) literature indicating a main tectonic phase during the end of the Miocene in the Gargano Promontory, and (iii) the occurrence of extensive Pleistocene and Holocene seismic-liquefaction features in the northern coastal area of Gargano are all independent sources of data that support the seismic origin for the described deformed layers.

The outcrop investigated in this study shows that SSDS are characterized by high lateral variability in terms of deformation pattern and thickness. This research highlights the concept that these changes are mostly determined by the pre-deformation sedimentary system and the driving force system acting during deformation. These findings should be taken into account when using SSDS for paleoseismic investigation at a basin-scale, and/or when analysing liquefaction events with the use of well cores and paleoseismic trenches,

because the number of deformed units and their main physical characters can change laterally.

Acknowledgments

The authors of this paper are grateful to the Editor Dr. Jasper Knight for his comments on the early drafts of the paper and to Dr.Gosia Pisarska-Jamrozy (Adam Mickiewicz University in Poland) and Dr Kari Bassett (Canterbury University, New Zealand) for their insightful revisions and comments for improving the readability of the paper.

REFERENCES

Alfaro, P., Gibert, L., Moretti, M., Garcia-Tortosa, F.J., de Galdeano, C.S., Galindo-Zaldivar, J., Lopez-Garrido, A.C., 2010. The significance of giant seismites in the Plio-Pleistocene Baza paleo-Lake (S Spain). Terra Nova 22, 172-179.

Allen, J.R.L., 1982. Sedimentary structures, their character and physical basis. Development in Sedimentology. Elsevier, New York.

Allen, J.R.L., Banks, N.L., 1986. An interpretation and analysis of recumbent-folded deformed cross-bedding. Sedimentology 19, 257-283.

Alsop, G.I., Marco, S., 2011. Soft-sediment deformation within seismogenic slumps of the Dead Sea Basin. Journal of Structural Geology 33, 433-457.

Anketell, J.M., Cegla, J., Dzulinsky, S., 1970. On the deformational structures in systems with reversed density gradients. Annales de la Société Géologique de Pologne 40, 3-30.

Argnani, A., Rovere, M., Bonazzi, C., 2009. Tectonics of the Mattinata fault, offshore south Gargano (southern Adriatic Sea, Italy): implications for active deformation and seismotectonics in the foreland of the Southern Apennines. Geological Society American Bulletin 121, 9-10.

Basher, D.J.A., Litchfield, N.J., Townsend, D.B., Quigley, M., Van Dissen, R.J., Cosgrove, R., Cox, S.C., Furlong, K., Villamor, P., Begg, J. G., Hemmings-Sykes, S., Jongens, R., Mackenzie, H., Noble, D., Stahl, T., Bilderback, E., Duffy, B., Henham, H., Klahn, A., Lang, E.M.W., Moody, L., Nicol, R., Pedley, K., Smith, A., 2011. Strike-slip ground surface rupture (Greendale Fault) associated with the 4 September 2010 Darfield Earthquake, Canterbury, New Zealand. Quarterly Journal of Engineering Geology and Hydrogeology 44, 283-291.

Bastin, S.H., Bassett, K., Quigley, M.C., Maurer, B., Green, R.A., Bradley, B., Jacobson, D., 2016. Late Holocene Liquefaction at Sites of Contemporary liquefaction during the 2010-2011 Canterbury Earthquake Sequence, New Zealand. Bullettin of the Seismological Society of America 106, 881-903.

Bathurst, R.G.C., 1983. Early Diagenesis of Carbonate Sediments. In: Parker, A., Sellwood, B.W. (Eds), Sediment Diagenesis. Proceedings NATO ASI Series book series 115 Reidel Publishing, pp. 349-378.

Bernoulli, D., 1972. North Atlantic and Mediterranean Mesozoic facies: a comparison. Initial Reports of the Deep Sea Drilling Project 11, 801-822.

Berra, F., Felletti, F., 2011. Syndepositional tectonics recorded by soft-sediment deformation and liquefaction structures(continental Lower Permian sediments, Southern Alps, Northern Italy): Stratigraphic significance. Sedimentary Geology 235, 249-263.

Bertotti, G., Casolari, E., Picotti, V., 1999. The Gargano Promontory: A Neogene contractional belt within the Adriatic plate. Terra Nova 11, 168-173.

Bertotti, G., Picotti, V., Chilovi, C., Fantoni, R., Merlini, S., Mosconi, A., 2001. Neogene to Quaternary sedimentary basins in the south Adriatic (central Mediterranean): Foredeeps and lithospheric buckling. Tectonics 20, 771-787.

Bezerra, F.H.R., Vita-Finzi, C., 2000. How active is a passive margin? Paleoseismicity in northeastern Brazil. Geology 28, 591–594.

Bhattacharya, H.N., Bandyopadhyay, S., 1998. Seismites in a Proterozoic tidal succession, Sinfhbhum, Bihar, India. Sedimentary Geology 119, 239-252.

Billi, A., Gambini, R., Nicolai, C., Storti, F., 2007. Neogene-Quaternary intraforeland transpression along a Mesozoic platform-basin margin: the Gargano fault system, Adria, Italy. Geosphere 3, https://doi.org/10.1130/GES00057.1

Borgomano, J.R.F., 2000. The Upper Cretaceous carbonates of the Gargano-Murge region, southern Italy: a model of platform-to-basin transition. American Association of Petroleum Geologists Bulletin 84, 1561-1588.

Borre, K., Cacon, S., Cello, G., Kontny, B., Kostak, B., Likke Andersen, H., Moratti, G., Piccardi, L., Stemberk, J., Tondi, E., Vilimek, V., 2003. The COST project in Italy: Analysis and monitoring of seismogenic faults in the Gargano and Norcia areas (central-southern Apennines, Italy). Journal of Geodynamics 36, 3–18.

Bosellini, A., Morsilli, M., Neri, C., 1999. Long-term event stratigraphy of the Apulia Platform margin (Upper Jurassic to Eocene, Gargano, southern Italy). Journal of Sedimentary Research 69, 1241–1252.

Bosellini, A., Neri, C., Luciani, V., 1993. Platform margin collapses and sequence stratigraphic organization of carbonate slopes: Cretaceous–Eocene, Gargano Promontory, southern Italy. Terra Nova 5, 282–297.

Brackley, H.L., Almond, P., Barrell, D.J., Begg, J., Berryman, K., Christensen, S., Dellow, G., Fraser, J., Grant, H., Harwood, N., Irwin, M., Jacka, M., Jones, K., Lee, J., McCahon, I., McMorran, T., Scott, D., Townsend, D., 2012. Review of liquefaction hazard information in eastern Canterbury, including Christchurch City and parts of Selwyn, Waimakariri and Hurunui Districts. GNS Science Consultancy Report 2012/218, 99 pp.

Brankman, C.M., Aydin, A., 2004. Uplift and contractional deformation along a segmented strike-slip fault system: the Gargano Promontory, southern Italy. Journal of Structural Geology 26, 807-824.

Cartwright, J.A., Dewhurst, D.N., 1988. Layer-bound compaction faults in fine-grained sediments. GSA Bulletin 110, 1245-1257.

Casolari, E., Negri, A., Picotti, V., Bertotti, G., 2000. Neogene stratigraphy and Sedimentology of the Gargano Promontory (Southern Italy) Eclogae Geologicae Helvetiae 93, 7-23.

Chiarella, D., Moretti, M., Longhitano, S.G., Muto, F., 2016. Deformed cross-stratified deposits in the Early Pleistocene tidally-dominated Catanzaro strait-fill succession, Calabrian Arc (Southern Italy): Triggering mechanisms and environmental significance. Sedimentary Geology 344, 277-289.

Chilovi, C., De Feyter, A., Pompucci, A., 2000. Wrench zone reactivation in the Adriatic Block: the example of the Mattinata Fault System (SE Italy). Bollettino della Società Geologica Italiana 119, 3-8.

Ciaranfi, N., Pieri, P., Ricchetti, G., 1988. Note alla carta geologica delle Murge e del Salento (Puglia centromeridionale). Memorie della Società Geologica Italiana 41, 449–460.

Cipollari, P., Cosentino, D. Gliozzi, E., 1999. Extension- and compression-related basins in central Italy during the Messinian Lago-Mare event. Tectonophysics 315, 163-185.

Cita, M.B., Wright, R. C., Ryan, W.B.F., Longinelli, A., 1978. Messinian paleoenvironments. In: Hsü, K.J., et al. (Eds), Initial Report of the Deep Sea Drilling Project 42, pp. 1003–1035.

Civico, R., Brunori, C.A., De Martini, P.M., Pucci, S., Cinti, F.R., Pantosti, D., 2015. Liquefaction susceptibility assessment in fluvial plains using airborne lidar: the case of the 2012 Emilia earthquake sequence area (Italy). Natural Hazards and Earth System Sciences 15, 2473-2483.

Clauzon, G., Suc, J.-P., Popescu, S.-M., Marunteanu, M., Rubino, J.-L., Marinescu, F., Melinte, M.C., 2005. Influence of the Mediterranean sea-level changes over the Dacic Basin (Eastern Paratethys) in the Late Neogene. The Mediterranean Lago Mare facies deciphered. Basin Research 17, 437-462.

Cosentino, D., Cipollari, P., Lo Mastro, S., Giampaolo, C., 2005. High-frequency cyclicity in the latest Messinian Adriatic foreland basin: Insight into palaeoclimate and palaeoenvironments of the Mediterranean Lago-Mare episode. Sedimentary Geology 178, 35-53.

D'Alessandro, A., Laviano, A., Ricchetti, G., Sardella, A., 1979. Il Neogene del Monte Gargano. Bollettino della Società Paleontologica Italiana 18, 9-116.

D'Argenio, B., 1976. Le piattaforme carbonatiche periadriatiche. Una rassegna di problemi nel quadro geodinamico mesozoico dell'area mediterranea. Memorie della Società Geologica Italiana 13, 137-159.

de Alteriis, G., 1995. Different foreland basins in Italy: Examples from the central and southern Adriatic Sea. Tectonophysics 252, 349-373.

De Dominicis, A., Mazzoldi, G., 1989. Interpretazione geologico-strutturale del margine orientale della piattaforma Apula. Memorie della Società Geologica Italiana 38, 163-176.

De Martini, P.M., Burrato, P., Pantosti, D., Maramai, A., Graziani, L., Abramson, H., 2003. Identification of tsunami deposits and liquefaction features in the Gargano area (Italy): paleoseismological implication. Annals of Geophysics 46, 883–902.

Del Gaudio, V., Pierri, P., Frepoli, A., Calcagnile, G., Venisti, N., Cimini, G.B., 2007. A critical revision of the seismicity of Northern Apulia (Adriatic microplate — Southern Italy) and implications for the identification of seismogenic structures. Tectonophysics 436, 9-35.

Deynoux, M., Proust, J.N., Durand, J., Merino, E., 1990. Water-transfer cylindrical structures in the Late Proterozoic eolian sandstone in the Taoudeni Basin, West Africa. Sedimentary Geology 66, 227-242.

Di Bucci, D., Ravaglia, A., Seno, S., Toscani, G., Fracassi, U., Valensise, G., 2006. Seismotectonics of the southern Apennines and Adriatic foreland: Insights on active regional E-W shear zones from analogue modeling. Tectonics 25, TC4015. doi.org/10.1029/2005TC001898

Dionne, J.C., 1973. Structures cylindriques verticales dans du Quaternaire a Athabaska, Quebec. Sedimentary Geology 9, 53-63.

Doglioni, C., Mongelli, F., Pieri, P., 1994. The Puglia uplift (SE Italy): An anomaly in the foreland of the Apenninic subduction due to buckling of a thick continental lithosphere. Tectonics 13, 1309–1321.

Dżułyński, S., Walton, E.K., 1965. Sedimentary Features of Flysch and Greywackes. Elsevier, Amsterdam. 273 pp.

Eberli, G.P., Bernoulli, D., Sanders, D., Vecsei, A., 1993. From aggradation to progradation: the Maiella Platform, Abruzzi, Italy. In: Simo, J.T., Scott, R.W., Masse, J.P. (Eds), Cretaceous Carbonate Platforms. American Association of Petroleum Geologists Memoir 56, pp. 213-232 .

EMERGEO, Working Group, 2013. Liquefaction phenomena associated with the Emilia earthquake sequence of May–June 2012 (Northern Italy). Natural Hazards and Earth System Sciences 13, 935–947.

Ezquerro, L., Moretti, M., Liesa, C.L., Luzón, A., Pueyo, E.L., Simón, J.L., 2016. Controls on space-time distribution of soft-sediment deformation structures: Applying palaeomagnetic dating to approach the apparent recurrence period of paleoseisms at the Concud Fault (eastern Spain). Sedimentary Geology 344, 91-111.

Ezquerro, L., Moretti, M., Liesa, C.L., Luzon, A., Simon, J.L., 2015. Seismites from a well core of palustrine deposits as a tool for reconstructing the paleoseismic history of a fault. Tectonophysics 655, 191-205.

Favali, P., Funiciello, R., Mattietti, G., Mele, G., Salvini, F., 1993. An active margin across the Adriatic Sea (Central Mediterranean Sea). Tectonophysics 219, 109-117.

Finetti, I., Bricchi, G., Dal Ben, A., Pipan, M., Ziyan, X., 1989. Geophysical study of the Adria Plate. Memorie Società Geologica Italiana 38, 335–344.

Fracassi, U., Di Bucci, D., Ridente, D., Trincardi, F. Valensise, G., 2012. Recasting Historical Earthquakes in Coastal Areas (Gargano Promontory, Italy) Insights from Marine Paleoseismology. Bulletin of the Seismological Society of America 102, 1-17.

Funiciello, R., Montone, P., Salvini, F., Tozzi, M., 1992. Caratteri strutturali del Promontorio del Gargano. Memorie della Società Geologica Italiana 41, 1235–1243.

Galli, P., 2000. New empirical relationshipts between magnitude and distance for liquefaction. Tectonophysics 324, 169-187.

Gambini, R., Tozzi, M., 1996. Tertiary evolution of the southern Adria microplate. Terra Nova 8, 593–602.

Giona Bucci, M., Villamor, P., Almond, P., Tutte, M., Ries, W., Smith, C., Hodge, M., Watson, M., 2018. Associations between sediment architecture and liquefaction susceptibility in fluvial settings: the 2010-2011 Canterbury Earthquake Sequence, New Zealand. Engineering Geology 237, 181-197.

Green, A.R., Maurer, B.W., Brendon, B., Wotherspoon, L., Cubrinovski, M., 2013. Implications from liquefaction observations in New Zealand for interpreting paleoliquefaction data in the central eastern united states (CEUS). U.S. Geological Society Final Technical Report, 97 pp.

Guerricchio, A., 1986. Strutture di blocco lungo la faglia trascorrente di Mattinata. Geologia Applicata e Idrogeologia 21, 25–36.

Guhman, A.I., Pederson, D.T., 1992. Boiling sand springs, Dismal River, Nebraska: agents for formation of vertical cylindrical structures and geomorphic change. Geology 20, 8–10.

Haczewski, G., 1996. Oligocene laminated limestone as a high-resolution correlator of Oligocene palaeoseismicity, Carpathians. In: Kemp, A.E.S. (Ed), Palaeoclimatology and Palaeoceanography from laminated Sediments. Geological Society Special Publication 116, pp. 209-220.

Henkel, D.J., 1970. The role of waves in causing submarine landslides. Geotechnique, 20, 75–80.

Hilbert-Wolf, H.L., Roberts, E.M., 2015. Giant Seismites and Megablock Uplift in the East African Rift: Evidence for Late Pleistocene Large Magnitude Earthquakes. PLoS ONE 10, https://doi.org/10.1371/journal.pone.0129051

Hilbert-Wolf, H.L., Simpson, E.L., Simpson, E.W., Tindall, S.E., Wizevich, M.C., 2009. Insights into syndepositional faultmovement in a foreland basin; trends in seismites of the Upper Cretaceous,Wahweap Formation,Kaiparowits Basin, Utah, USA. Basin Research 21, 856-871.

Holzer, T.M., Clark, M.M., 1993. Sand boils without earthquakes. Geology 21, 873-876.

Hornblow, S., Quigley, M., Nicol, A., Van Dissen, R., Wang, N., 2014. Paleoseismology of the 2010 Mw 7.1 Darfield (Canterbury) earthquake source, Greendale Fault, New Zealand. Tectonophysics 637, 178-190.

Idriss, I.M., Boulanger, R.W., 2006. Semi-empirical procedures for evaluating liquefaction potential during earthquakes. Soil Dynamics and Earthquake Engineering 26, 115-130.

Jones, A., Omoto, K., 2000. Towards establishing criteria for the identifying trigger mechanisms for soft-sediment deformation: a case study of Late Pleistocene lacustrine sands and clays, Onikobe and Nakayamadaira Basins, northeastern Japan. Sedimentology 47, 1211-1226.

Kuenen, P.H., 1958. Experiments in geology. Transactions of the Geological Society of Glasgow 23, 1-28.

Leeder, M.R., 1987. Sediment deformation structures and the palaeotectonic analysis of sedimentary basins, with a case-study from the Carboniferous of northern England. In: Jones, M.E. and Preston, R.M.F. (Eds), Deformation of Sediments and Sedimentary Rocks. Geological Society Special Publication London 29, pp. 137–146.

Lowe, D.R., 1975. Water escape structures in coarse-grained sediments. Sedimentology 22, 157-204.

Masse, J., Luperto Sinni, E., 1989. A platform to basin transitional model: the Lower Cretaceous carbonates of the Gargano Massif. Memorie della Società Geologica Italiana 40, 99-108.

Mastrogiacomo, G., Moretti, M., Owen, G., Spalluto, L., 2012. Tectonic triggering of slump sheets in the Upper Cretaceous carbonate succession of the Porto Selvaggio area (Salento peninsula, southern Italy): Synsedimentary tectonics in the Apulian Carbonate Platform. Sedimentary Geology 269-270, 15-27.

Méhes, G., 1908. Ostracod Ungarns: In: Pioz, B.Z.K.D. (Ed), Die Darvinulidaeen und Cytheridaeen d. unterpannonischen Stufe. Suppl. Z. Földt. Közl. 38, S., Taf. 8-11, Budapest, pp. 601-635.

Milano, G., Di Giovambattista, R., Ventura, G., 2005. Seismic constraints on the present-day kinematics of the Gargano foreland, Italy, at the transition zone between the southern and northern Apennine belts. Geophysical Research Letters 32, L24308, doi.org/10.1029/2005GL024604

Mohindra, R., Bagati, T.N., 1996. Seismically induced soft-sediment deformation structures (seismites) around Sumdo in the lower Spiti valley (Tethys Himalaya). Sedimentary Geology 101, 69-83.

Molina, J.M., Alfaro, P., Moretti, M., Soria, J.M., 1998. Soft-sediment deformation structures induced by cyclic stress of storm waves in tempestites (Miocene, Guadalquivir Basin, Spain). Terra Nova 10, 145–150.

Montenat, C., d'Estevou, O., Barrier, P., Paturel, D., 1993. Les séismites: essai de typologie génétique. Géocronique 46, 15-17.

Moretti, M., 2000. Soft-sediment deformation structures interpreted as seismites in middle-late Pleistocene aeolian deposits (Apulian foreland, southern Italy). Sedimentary Geology 135, 167-179.

Moretti, M., Alfaro, P., Caselles, O., Canas, J.A., 1999. Modelling seismites with a digital shaking table. Tectonophysics 304, 369-383.

Moretti, M., Alfaro, P., Owen, G., 2016. The environmental significance of soft-sediment deformation structures: key signatures for sedimentary and tectonic processes. Sedimentary Geology 344, 1-4.

Moretti, M., Pieri, P., Ricchetti, G., Spalluto, L., 2011. Note Illustrative della Carta Geologica d'Italia alla scala 1: 50.000 Foglio 396 'San Severo', ISPRA Servizio Geologico d'Italia.

Moretti, M., van Loon, A.J.T., 2014. Restrictions to the application of 'diagnostic' criteria for recognizing ancient seismites. Journal of Palaeogeography 3, 162-173.

Morsilli, M., 2005. Soft-sediment deformation structures in the Lago-Mare unit (Late Messinian, Gargano Promontory, Apulia, southern Italy). Geoitalia, 5 forum italiano di Scienze della Terra, Spoleto.

Morsilli, M., 2016. Sintesi delle conoscenze geologiche e stratigrafiche del promontorio del Gargano, Geologi e Territorio. Ordine Regionale dei Geologi Puglia 2, 15-30.

Morsilli, M., Bosellini, A., 1997. Carbonate facies zonation of the Upper Jurassic–Lower Cretaceous Apulia Platform Margin (Gargano Promontory, southern Italy). Rivista Italiana di Paleontologia e Stratigrafia 103, 193-206.

Morsilli, M., Bosellini, A., Neri, C., 2017. Note illustrative della carta geologica d'Italia alla scala 1:50.000, Foglio 384 Vico del Gargano, APAT Servizio Geologico d'Italia.

Morsilli, M., Moretti, M., 2009. Soft-sediment deformation structures in a tidal-dominated lagoonal deposits of the Gargano Promontory (late Messinian?, Apulia, southern Italy). 27th IAS Meeting of Sedimentology, Alghero, 612.

Obermeier, S.F., 1996. Use of liquefaction-induced features for paleoseismic analysis- An overview of how seismic liquefaction feature can be distinguished from other feature and how their regional distribution and properties of source sediment can be used to infer the location and strength of Holocene paleo-earthquakes. Engineering Geology 44, 1-76.

Obermeier, S.F., Pond, E.C., Olson, S.M., Green, R.A., 2002. Paleoliquefaction studies in continental settings. In:Ettensohn, F.R., Rast, N., Brett, C.E. (Eds), Ancient seismites. Geological Society of America Special Paper 359, 13-27.

Olson, S.M., Green, R.A., Obermeier, S.F., 2005a. Field occurrences of liquefaction induced features: a primer for engineering and geologic analysis of paleoseismic shaking. Engineering Geology 76, 209-234.

Olson, S.M., Russell, A. G., Obermeier, S.F., 2005b. Revised Magnitude-bound Relation for the Wabash Valley Seismic Zone of the Central United States. Seismological Research Letters 76, https://doi.org/10.1785/gssrl.76.6.756

Onofrio, V., Tropeano, M., Festa, V., Moretti, M., Sabato, L., 2009. Quaternary transpression and lacustrine sedimentation in the San Lorenzo area (Sant'Arcangelo Basin, Italy). Sedimentary Geology 222, 78-88.

Orszagsperber, F., 2006. Changing perspectives in the concept of “Lago-Mare” in Mediterranean Late Miocene evolution. Sedimentary Geology 188-189, 259-277.

Ortolani, F., Pagliuca, S., 1989. Tettonica transpressiva nel Gargano e rapporti con le catene appenninica e dinarica. Memorie della Società Geologica Italiana 38, 205-220.

Owen, G., 1987. Deformation Processes in unconsolidated sands. In: Jones, M.E., Preston, R.M.F. (Eds), Geological Society of London, Special Publications 29, 11-24.

Owen, G., 1996a. Anatomy of a water-escape cusp in the Upper Proterozoic Torridon Group sandstones, Scotland. Sedimentary Geology 103, 117-128.

Owen, G., 1996b. Experimental soft-sediment deformation: structures formed by the liquefaction of unconsolidated sands and some ancient examples. Sedimentology 43, 279-293.

Owen, G., 2003. Load structures: gravity-driven sediment mobilization in the shallow subsurface. In: Van Rensbergen, P., Hillis, R.R., Maltman, A.J., Morley, C.K.J. (Eds), Subsurface Sediment Mobilization. Geological Society Special Publications London 216, pp. 21-34.

Owen, G., Moretti, M., 2008. Determining the origin of soft-sediment deformation structures: a case study from Upper Carboniferous delta deposits in south-west Wales, UK. Terra Nova 20, 237-245.

Owen, G., Moretti, M., 2011. Identifying triggers for liquefaction-induced soft-sediment deformation in sands. Sedimentary Geology 235, 141-147.

Owen, G., Moretti, M. , Alfaro, P., 2011. Recognising triggers for soft sediment deformation: current understanding and future directions. Sedimentary Geology 235, 133-140.

Patacca, E., Scandone, P., 2004. The 1627 Gargano earthquake (southern Italy): Identification and characterization of the causative fault. Journal of Seismology 8, 259 -273.

Piccardi, L., 2005. Paleoseismic evidence of legendary earthquakes: the apparition of Archangel Michael at Monte Sant'Angelo (Italy). Tectonophysics 408, 113-128.

Pisarska-Jamroży, M., Belzyt, S., Bitinas, A., Jusienė, A., Woronko, B., 2019. Seismic shocks, periglacial conditions and glaciotectonics as causes of the deformation of a Pleistocene meandering river succession in central Lithuania. Baltica 32, 63-77.

Pisarska-Jamroży, M., Paweł, P., 2019. Debris flow and glacioisostatic-induced soft-sediment deformation structures in a Pleistocene glaciolacustrine fan: The southern Baltic Sea coast, Poland. Geomorphology 326, 225-238.

Quigley, M., Van Dissen, R., Litchfield, N., Villamor, P., Duffy, B., Barrell, D., Furlong, K., Stahl, T., Bilderback, E., Noble, D., 2012. Surface rupture during the 2010 Mw 7.1 Darfield (Canterbury) earthquake: implications for fault rupture dynamics and seismic-hazard analysis. Geology 40, 55-58.

Quigley, M.C., Hughes, M.W., Bradley, B.A., van Ballegooy, S., Reid, C.M., Morgenroth, J., Horton, T.W., Duffy, B., Pettinga, J.R., 2016. The 2010-2011 Canterbury earthquake sequence: Environmental effects, seismic triggering thresholds and geologic legacy. Tectonophysics 672, 228-274.

Ridente, D., Trincardi, F., 2006. Active foreland deformation evidenced by shallow folds and faults affecting late Quaternary shelf-slope deposits (Adriatic Sea, Italy). Basin Research 18, 171-188.

Robledo, P. , Pomar, L., 2000. Upper Miocene karst collapse structures of the east coast, Mallorca, Spain. Acta Carsologica 2, 177–185.

Rodríguez-López , J.P., Meléndez, N., Soria, A.R., Liesa, C.L., van Loon, A.J.T., 2007. Lateral variability of ancient seismites related to differences in sedimentary facies (the synrift Escucha Formation, mid-Cretaceous, eastern Spain). Sedimentary Geology 201, 461–484.

Rodriguez Pascua, M.A., Calvo, J.P., De Vincente, G., Gomez- Gras, D., 2000. Soft-sediment deformation structures interpreted as seismites in lacustrine sediments of the Prebetic Zone, SE Spain, and their potential use as indicators of earthquake magnitudes during the Late Miocene. Sedimentary Geology 135, 117-135.

Rossetti, D.F., Santos Jr., A.E., 2003. Events of sediment deformation and mass failure in Upper Cretaceous estuarine deposits (Cametá Basin, northern Brazil) as evidence for seismic activity. Sedimentary Geology 161, 107-130.

Roveri, M., Flecker, R., Krijgsman, W., Lofi, J., Lugli, S., Manzi, V., Sierro, F.J., Bertini, A., Camerlenghi, A., De Lange, G., Govers, R., Hilgen, F.J., Hübscher, C., Meijer, P.T., Stoica, M., 2014. The Messinian salinity crisis: past and future great challenge for marine sciences. Marine Geology 352, 25-58

Ruggieri, G., 1967. The Miocene and later evolution of the Mediterranean Sea. In: Adams, C.G., Ager, D.V. (Eds), Aspects of Tethyan Biogeography. Publication of the Systematic Association 1967/7, pp. 283-290.

Salvini, F., Billi, A. Wise, D.U., 1999. Strike-slip fault propagation cleavage in carbonate rocks: The Mattinata fault zone. Journal of Structural Geology 21, 1731–1749.

Schneiderhan, E.A., Bhattacharya, H.N., Zimmermann, U., Gutzmer, J., 2005. Archean seismites of the Ventersdorp Supergroup, South Africa. South African Journal of Geology 108, 345-355.

Seilacher, A., 1969. Fault-graded beds interpreted as seismites. Sedimentology 13, 155-159.

Sims, J.D., 1975. Determining earthquake recurrence intervals from deformational structures in young lacustrine sediments. Tectonophysics 29, 141-152.

Spalluto, L., Moretti, M., 2006. Evidenze di neotettonica (Pliocene medio-Pleistocene superiore) nel settore occidentale del Promontorio del Gargano (Italia meridionale). Italian Journal of Quaternary Sciences 19, 143-154.

Spalluto, L., Moretti, M., Festa, V., Tropeano, M., 2007. Seismically-induced slumps in Lower-Maastrichtian peritidal carbonates of the Apulian Platform (southern Italy). Sedimentary Geology 196, 81-98.

Talwani, P., Amick, D., 1995. Study of paleoliquefaction features for seismic hazard assessment. In: Valensise, G., Pantosti, D., (Eds.), Active Faulting Studies for Seismic Hazard Assessment.International School of Solid Earth Geophysics 11th Course, Erice-Sicily, pp. 1-9.

Tondi, E., Piccardi, L., Cacon, S., Kontny, B., Cello, G., 2005. Structural and time constraints for dextral shear along the seismogenic Mattinata fault (Gargano, southern Italy). Journal of Geodynamics 40, 134-152.

Tuttle, M., 2001. The use of liquefaction features in paleoseismology : lessons learned in the New Madrid Seismic Zone, central United States. Journal of Seismology 5, 361-380.

Tuttle, M., Barstow, N., 1996. Liquefaction-related ground failure: a case study in the New Madrid Seismic Zone, Central United States. Bullettin of the Seismological Society of America 86, 636-645.

Tuttle, M.P., Hartleb, R., Wolf, L., Mayne, P.W., 2019. Paleoliquefaction studies and the evaluation of Seismic Hazard-review. Geosciences 9, 61.,https://doi.org/10.3390/geosciences9070311

Tuttle, M.P., Schweig, E.S., Sims, J.D., Lafferty, R.H., Wolf, L.W., Haynes, M.L., 2002. The earthquake potential of the New Madrid Seismic Zone. Bullettin of the Seismological Society of America 92, 2080-2089.

Tuttle, M.P., Villamor, P., Almond, P., Bastin, S., Giona Bucci, M., Langdridge, R., Clark, K., Hardwick, C., 2017. Liquefaction induced by the 2010-2011 Canterbury, New Zealand, Eartquake Sequence and Lessons Learned for the Study of Paleoliquefaction features. Seismological Research Letters 88, https://doi.org/10.1785/0220170073

Valenzano, E., Scardino, G., Cipriano, G., Fago, P., Capolongo, D., De Giosa, F., Lisco, S., Mele, D., Moretti, M., Mastronuzzi, G., 2018. Holocene morpho-sedimentary evolution of the Mar Piccolo basin (Taranto, Southern Italy). Geografia Fisica e Dinamica Quaternaria 41, 119-135.

van Bellegooy, S., Cox, S.C., Agnihotri, R., Reynolds, T., Thurlow, C., Rutter, H.K., Scott, D.M., Begg, J.G., McCahon, I., 2014. Median water table elevation in Christchurch and surroundings area after the 4 September 2010 Darfield Earthquake (version 2). GNS Science consultancy report 2013/1, 79 pp. + appendices.

Van Dissen, R., Barrel, D., Licthfield, N., Villamor, P., Quigley, M., 2011. Surface rupture displacement on the Greendale Fault during the Mw7.1 Darfield (Canterbury) earthquake, New Zealand, and its impact on man-made structures. In: NZSEE (Editor), Ninths Pacific Conference on Earthquake Engineering, Auckland, New Zealand, 14-16 April, 186.

Villamor, P., Almond, P., Tuttle, M.P., Giona Bucci, M., Langridge, R.M., Clark, K., Ries, W., Bastin, S.H., Eger, A., Vandergoes, M., Quigley, M.C., Barker, P., Martin, F. Howarth, J., 2016. Liquefaction features produced by the 2010-2011 Canterbury earthquake sequence in southwest Christchurch, New Zealand and preliminary assessment of paleoliquefaction features. Bulletin of Seismological Society of America 106, 1747–1771.

Wheeler, R.L., 2002. Distinguishing seismic from nonseismic soft-sediment structures: Criteria from seismic-hazard analysis. In: Ettensohn, F.R., Rast, N., Brett, C. E. (Eds), Ancient seismites. Geological Society of America Special Paper 353, pp. 1-11.

Youd, T.L., 2001. Liquefaction Resistance of soils: summary report from the 1996 NCEER and 1998 NCEER/ NSF Workshop on Evaluation of Liquefaction Resistance of Soils. Journal of Geotechnical and Geoenvironmental Engineering 127, 817-833.

FIGURE CAPTIONS

Fig. 1. Simplified geological map of the northern Apulia and Adriatic Sea. The Gargano Promontory is characterized by faults with different kinematic. The most preeminent features are the structural highs of the Tremiti Islands and the Mattinata Fault, a strike slip fault that passes offshore to the Gondola line (modified after Morsilli et al., 2017). The study area (Fig. 2) is indicated in a small green box.

Fig. 2. Geological map of the study area where the "calcari di Fiumicello" and other stratigraphic units crop out (modified after Morsilli et al., 2017). Stratigraphic logs have been documented along three railroad trenches.

Fig. 3. Sedimentological and stratigraphical logs with their location. Five deformed layers (SSDS) were observed in Trench 1, six in Trench 2, and five in Trench 3.

Fig. 4. Deformed units in the Trench I. (**A**). The deformed Unit A is characterised by ball-and-pillows surrounded by massive sediments. Note the presence of deformed laminae within the inner portion of the pillows in the top-right-hand corner of the frame. (**B**)**.** Flame structures separate adjacent load-structures in the deformed Unit B. (**C**). The deformed Unit C shows lateral variations: a single deformed unit (C) passes laterally to two thinner deformed unit (C_1 and C_2). (**D**). Load-structures of the deformed Unit D. (**E**)**.** Folds like structures in the deformed Unit E. Note the presence of breccia and compressional features in the whitish laminae.

Fig. 5. Deformed units in Trench 2. (**A**). The deformed units F, G and H occur in the lower portion of calcarenite beds and are represented by tight load-structures. (**B**). The deformed unit I contains load-structures with preserved primary lamination, (pen for a scale). (**C**). Panoramic view of L and M deformed units. Note that they are separated by an undeformed thin layer. Small-scale faults involve both deformed units and the displacement seems to end upward in the upper part of the deformed unit M. These faults are oriented dip direction N30, and N200. (**D**). The deformed unit L is characterized by complex of load-structures (ball-and-pillows) locally cross-cut by upward-directed laminae. (**E**). A set of tight folds (blue arrows) occurs just above the undeformed layer that separates L and M deformed units, involving the basal portion of the deformed unit M. Note the top section of unit M shows chaotic and fragmented laminae/layers. (**F**). Example of an irregular fold within the intermediate portion of the deformed unit M, pen for a scale. A Rose diagram shows the dip

direction of the fold axial planes (17 measurements). Data are very scattered, but seem to show a rough preferential orientation of axial planes dip directions toward W and SW, partially in agreement with the main synsedimentary faults (see Fig. 5C)

Fig. 6. Deformed units in Trench 3. (**A**). The deformed unit N shows narrow load structures and it occurs just below foresets in medium- and coarse-grained calcarenites. (**B**). Photo and sketch of the deformed unit O. Note that large load-structures formed at the interface (in blue) between massive whitish silt and the overlying coarse-grained calcarenites in foresets. (**C**). The deformed unit P occurs along the foresets (in orange the direction of their migration) and shows slump or breccia features. (**D**). Two details of the deformed unit Q. Load structures with preserved lamination. (**E**). Photo/sketch of the deformed bed R. Load-structures with complex internal lamination (IL) are separated by upward-directed features. The sediment surrounding adjacent load-structures is homogenised and massive (HMS) and primary lamination is not preserved.

Fig. 7. Schematic model summarising the three types of lateral variations observed at our study site. (**A**). Lateral variation of Type 1 is characterised by a reduced length, and is mainly associated with overloading, unequal loading and slump occurrence. (**B**). In the lateral variation of Type 2, style and/or thickness of the deformed units laterally changes along several meters until disappearing. (**C**)**.** In the lateral variation of Type 3, SSDS affect the whole thickness of a layer that laterally passes in two deformed and thinner sub-layers.

Fig. 8. Trench 2. Tectonics involving the deformed units. The scale of the displacement in the small-scale graben can be appreciated observing the top of the deformed unit L. Synsedimentary activity is recorded within the deformed unit M, which seems to increase its thickness in the hanging-wall portion of the graben.

Fig. 9. A neptunian dyke occurred in Trench 2. Note that the infill coming from the upper sedimentary units is made up of well-rounded pebbles.

Fig. 10. Microphotographs showing grains from load structures derived from the deformed bed H (Trench 2). At the end of the liquefaction process, the top and denser unit will sink into the bottom unit, with lower density.

The bottom unit will tend to move upward to re-establish a system that is more stable in the field of gravity. Photos taken using crossed nicols.

Fig. 11. Interpretation on the dynamics of the deformed unit C. Scenario 1 is the solution suggested in this paper. A single event induces a bifurcation of the deformed bed because of the occurrence of a permeability barrier which is variable in thickness and represented by the layer Uc. Scenario 2 implies the deformation of an older unit, the formation of an erosional surface, and then a later phase of sedimentation with a further final deformation occurring within the younger unit. The final geometry is similar to the Scenario 1, but two deformation events are needed. Scenario 3 leads to the same final geometry providing three deformation events being different the succession of sedimentary and erosional phases.

UNIVERSITÀ DEGLI STUDI DI BARI ALDO MORO

DIPARTIMENTO DI SCIENZE DELLA TERRA E GEOAMBIENTALI
DOTTORATO IN GEOSCIENZE

of
Sedimentary Geology

D

Bari, 2

.....
etti)

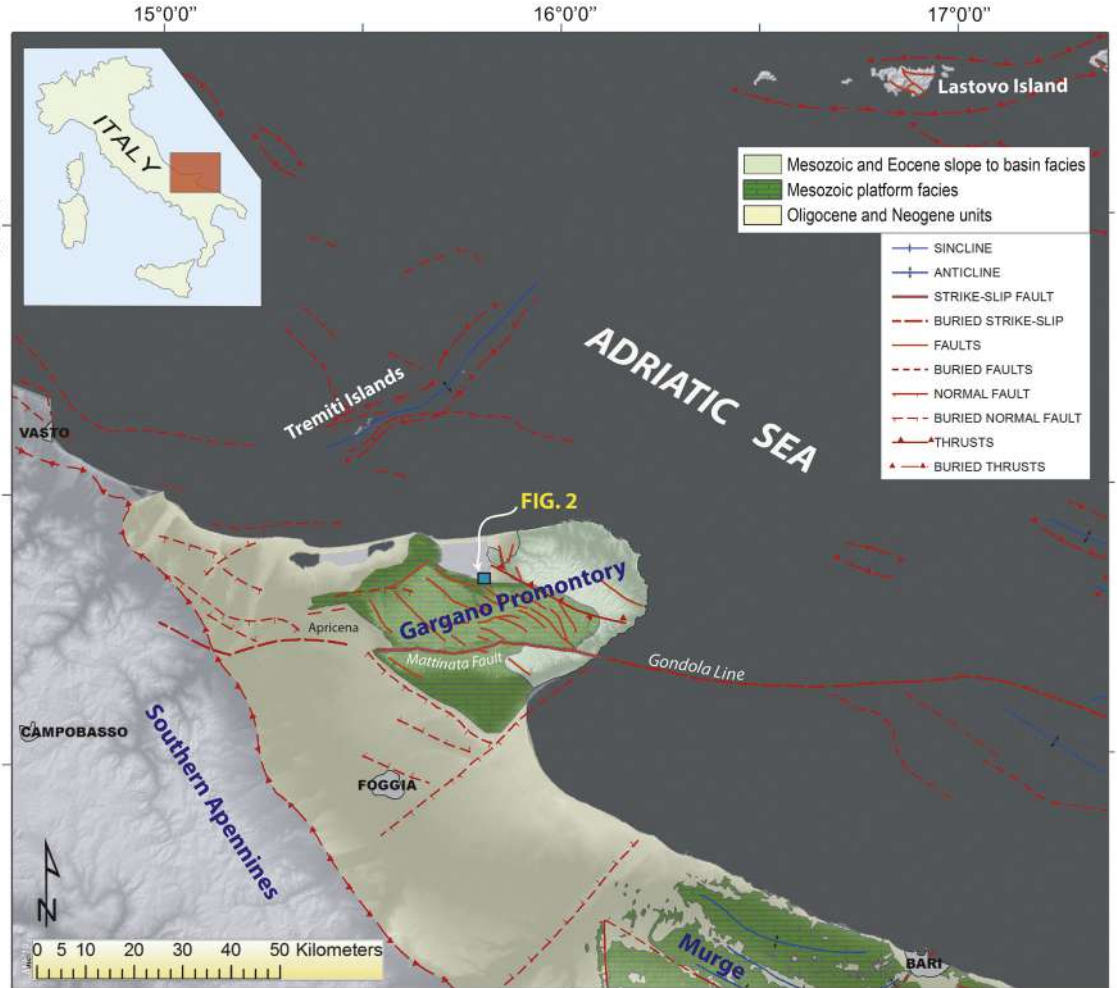
15°0'0"
16°0'0"
17°0'0"
42°30'0"
42°0'0"
41°30'0"
ITALY
Lastovo Island
Mesozoic and Eocene slope to basin facies
Mesozoic platform facies
Oligocene and Neogene units
SINCLINE
ANTICLINE
STRIKE-SLIP FAULT
BURIED STRIKE-SLIP
FAULTS
BURIED FAULTS
NORMAL FAULT
BURIED NORMAL FAULT
THRUSTS
BURIED THRUSTS
ADRIATIC SEA
Tremiti Islands
VASTO
FIG. 2
Gargano Promontory
Apricena
Mattinata Fault
Gondola Line
CAMPOBASSO
Southern Apennines
FOGGIA
Murge
BARI
N
0 5 10 20 30 40 50 Kilometers

Figure 1

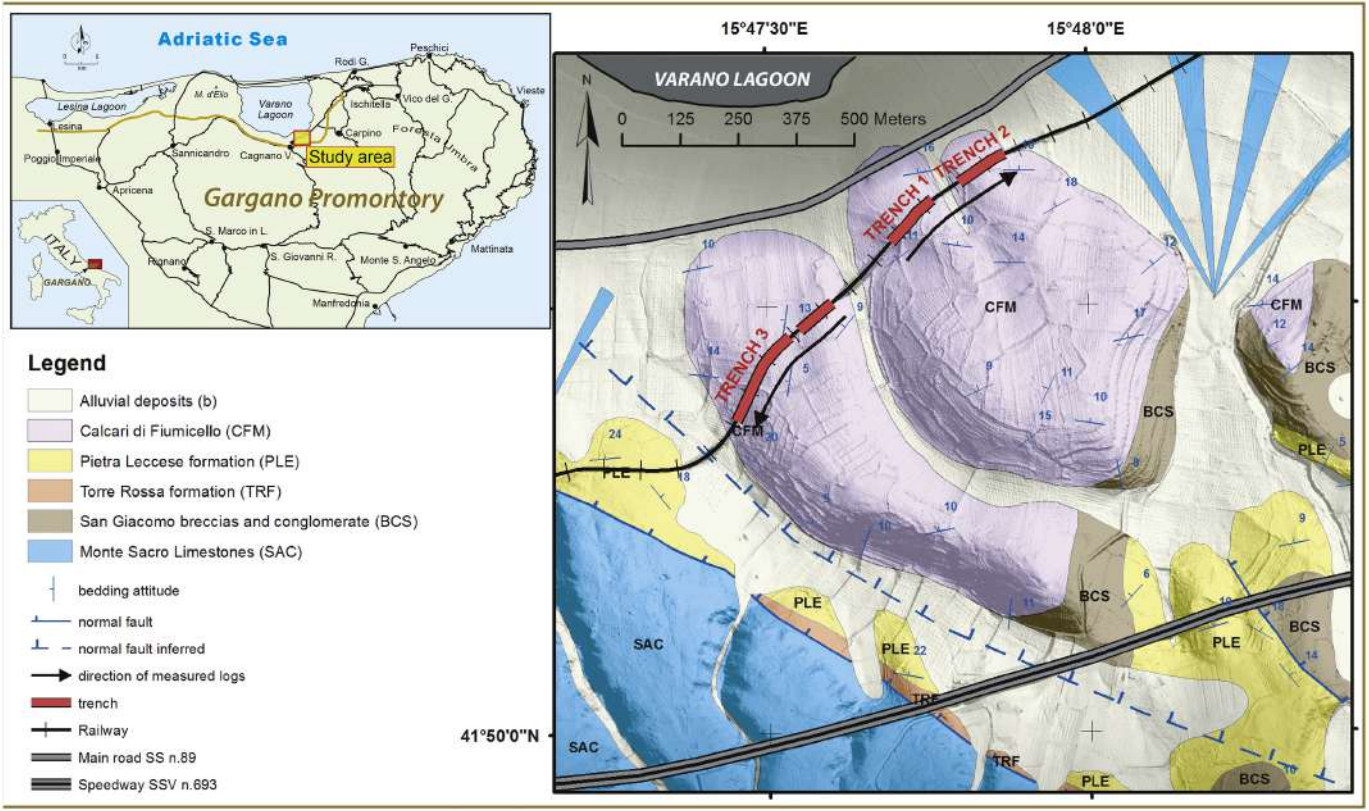
Adriatic Sea
Rodi G.
Peschici
Vieste
Lesina Lagoon
M. d'Elio
Varano Lagoon
Ischitella
Vico del G.
Lesina
Carpino
Foresta Umbra
Poggio Imperiale
Sannicandro
Cagnano V.
Study area
Apricena
Gargano Promontory
S. Marco in L.
ITALY
GARGANO
Rignano
S. Giovanni R.
Monte S. Angelo
Mattinata
Manfredonia
15°47'30"E
15°48'0"E
VARANO LAGOON
N
0 125 250 375 500 Meters
TRENCH 1
TRENCH 2
TRENCH 3
CFM
BCS
PLE
SAC
TRF
41°50'0"N
Legend
Alluvial deposits (b)
Calcari di Fiumicello (CFM)
Pietra Leccese formation (PLE)
Torre Rossa formation (TRF)
San Giacomo breccias and conglomerate (BCS)
Monte Sacro Limestones (SAC)
bedding attitude
normal fault
normal fault inferred
direction of measured logs
trench
Railway
Main road SS n.89
Speedway SSV n.693

Figure 2

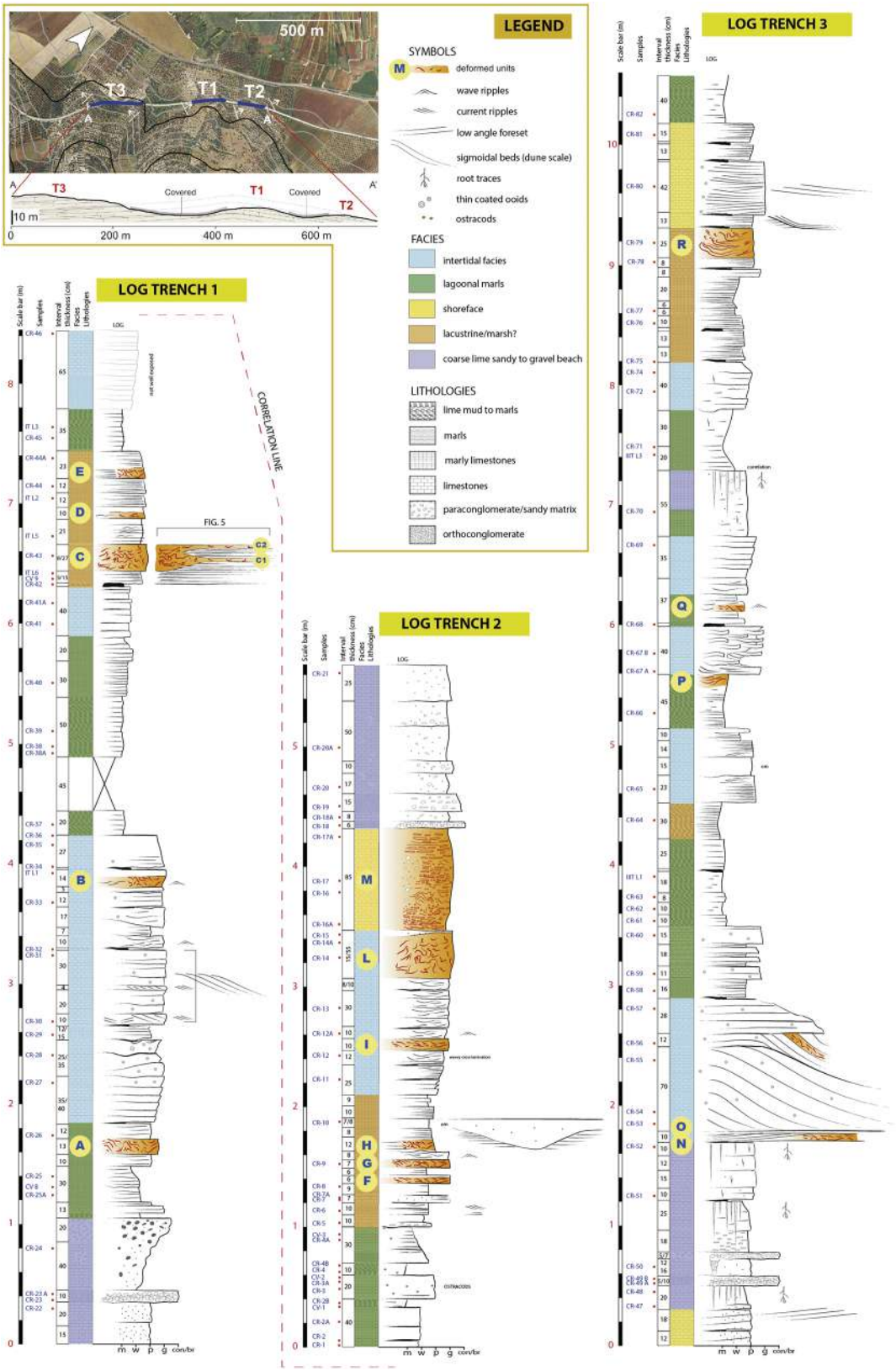
500 m
T3
T1
T2
A
A'
Covered
Covered
10 m
0
200 m
400 m
600 m
LEGEND
SYMBOLS
M
deformed units
wave ripples
current ripples
low angle foreset
sigmoidal beds (dune scale)
root traces
thin coated ooids
ostracods
FACIES
intertidal facies
lagoonal marls
shoreface
lacustrine/marsh?
coarse lime sandy to gravel beach
LITHOLOGIES
lime mud to marls
marls
marly limestones
limestones
paraconglomerate/sandy matrix
orthoconglomerate
LOG TRENCH 1
LOG TRENCH 2
LOG TRENCH 3
CORRELATION LINE
FIG. 5
C2
C1
Scale bar (m)
Samples
Interval thickness (cm)
Facies
Lithologies
LOG
m w p g con/br

Figure 3

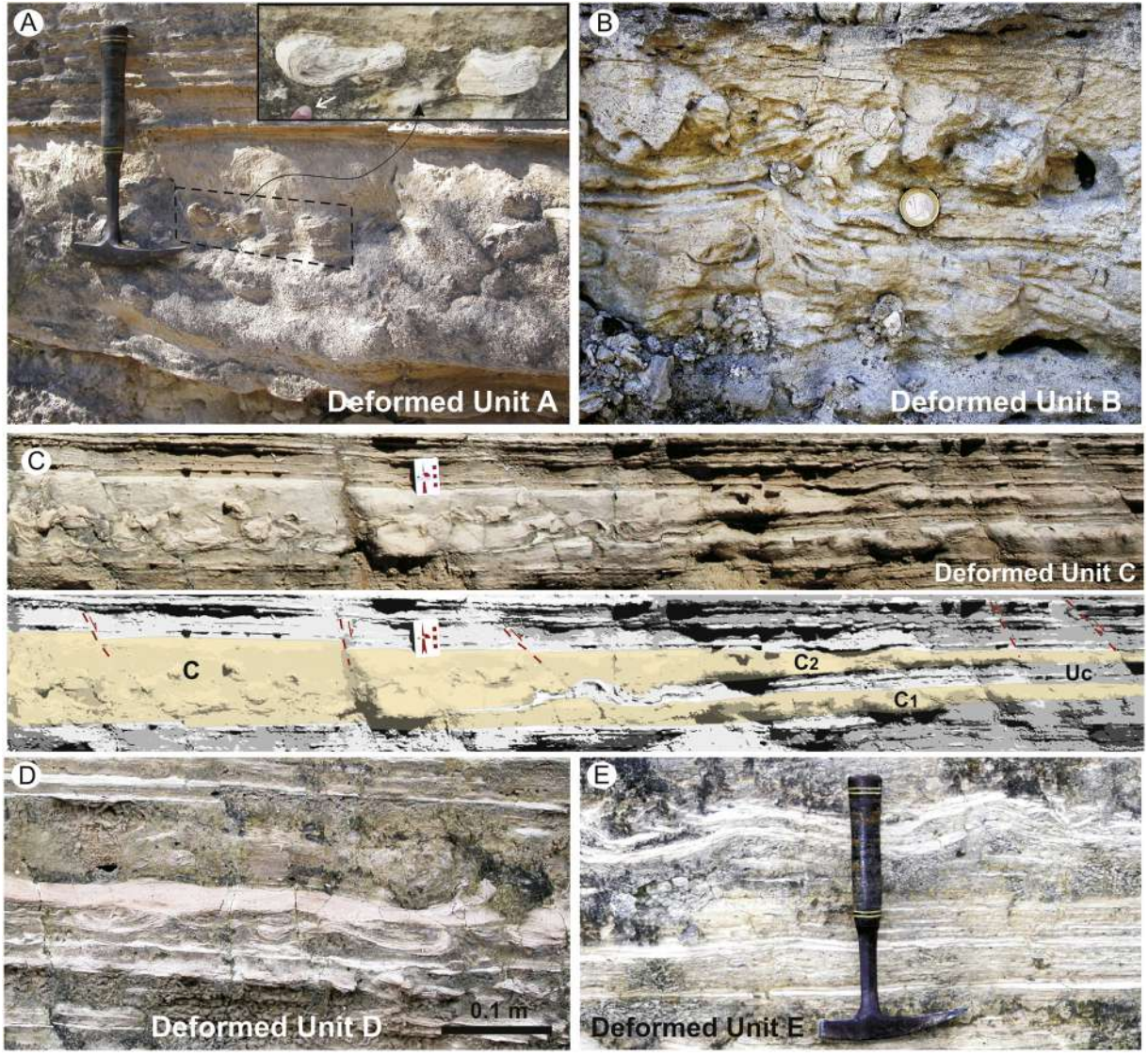
A
Deformed Unit A
B
Deformed Unit B
C
Deformed Unit C
C
C2
C1
Uc
D
Deformed Unit D
0.1 m
E
Deformed Unit E

Figure 4

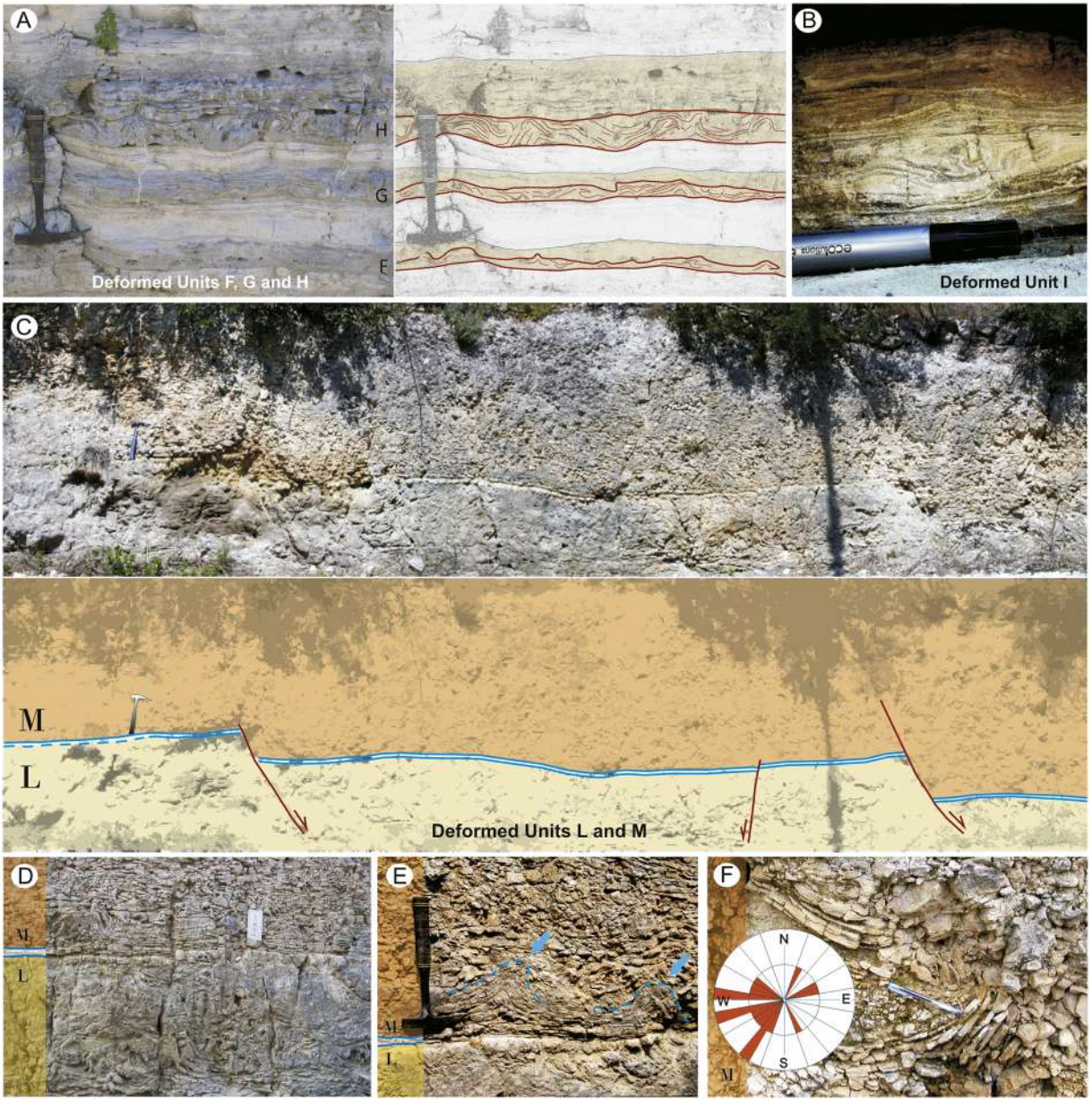
A
H
G
F
Deformed Units F, G and H
B
Deformed Unit I
C
M
L
Deformed Units L and M
D
M
L
E
M
L
F
N
W
E
S
M

Figure 5

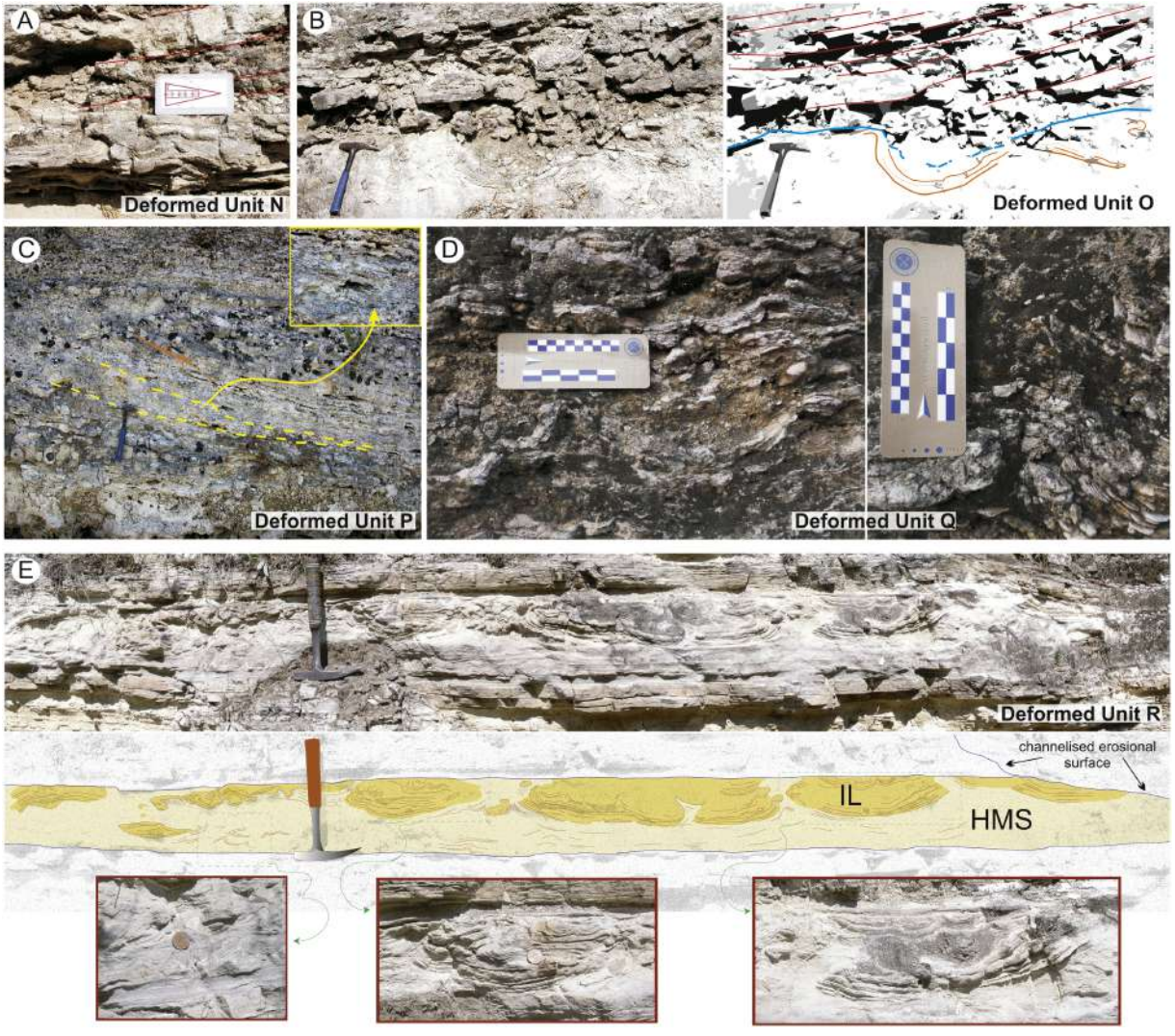
A
Deformed Unit N
B
Deformed Unit O
C
Deformed Unit P
D
Deformed Unit Q
E
Deformed Unit R
channelised erosional surface
IL
HMS

Figure 6

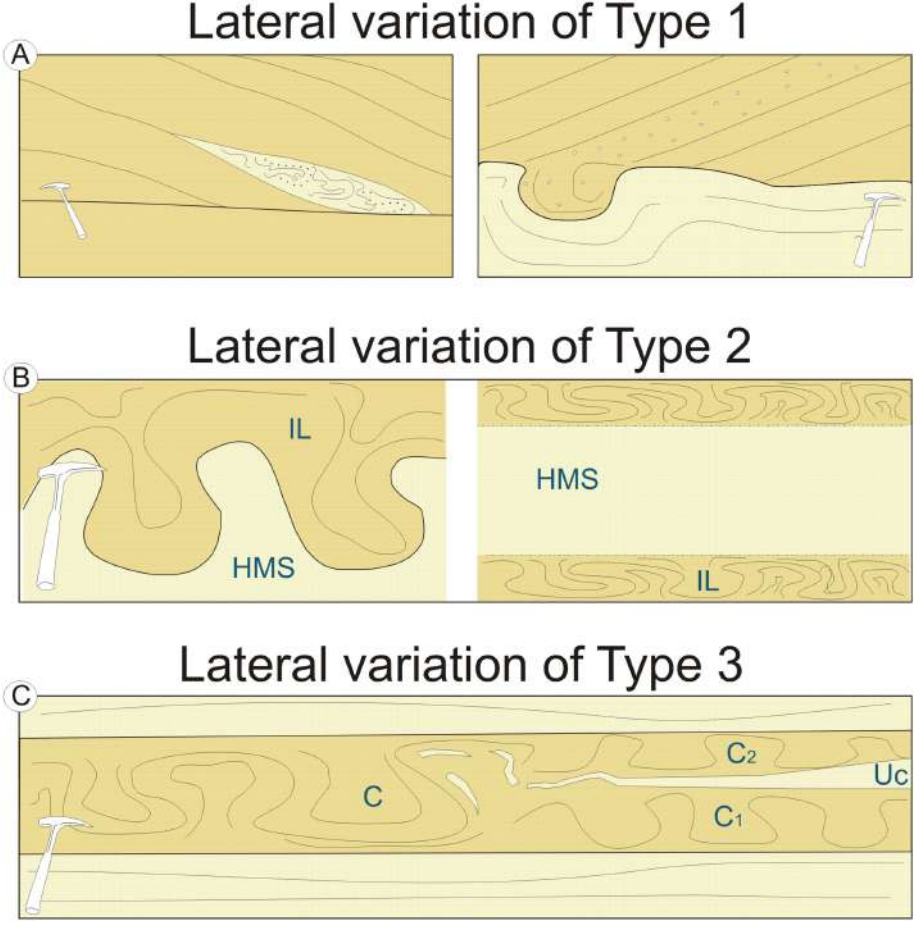
Lateral variation of Type 1
A
Lateral variation of Type 2
B
IL
HMS
HMS
IL
Lateral variation of Type 3
C
C
C2
Uc
C1

Figure 7

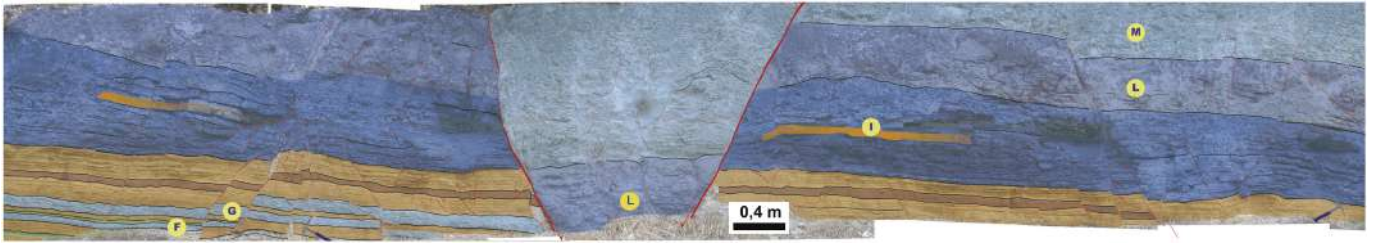

Figure 8

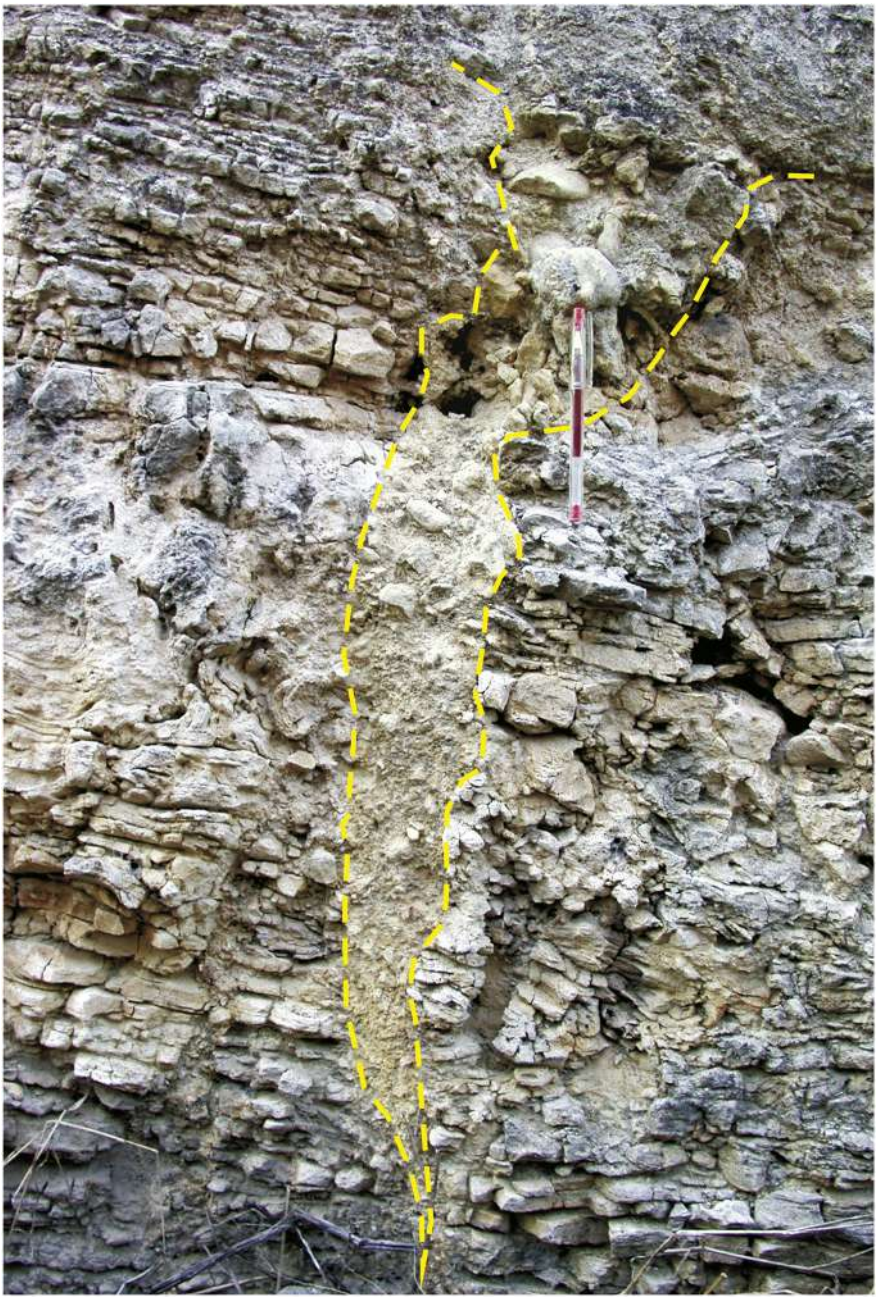

Figure 9

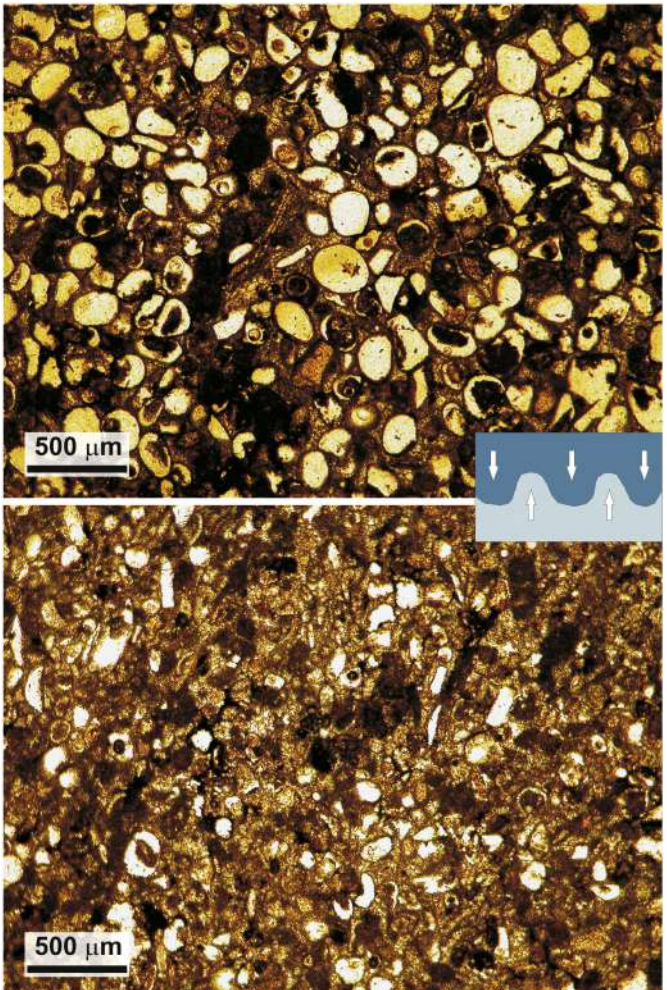

Figure 10

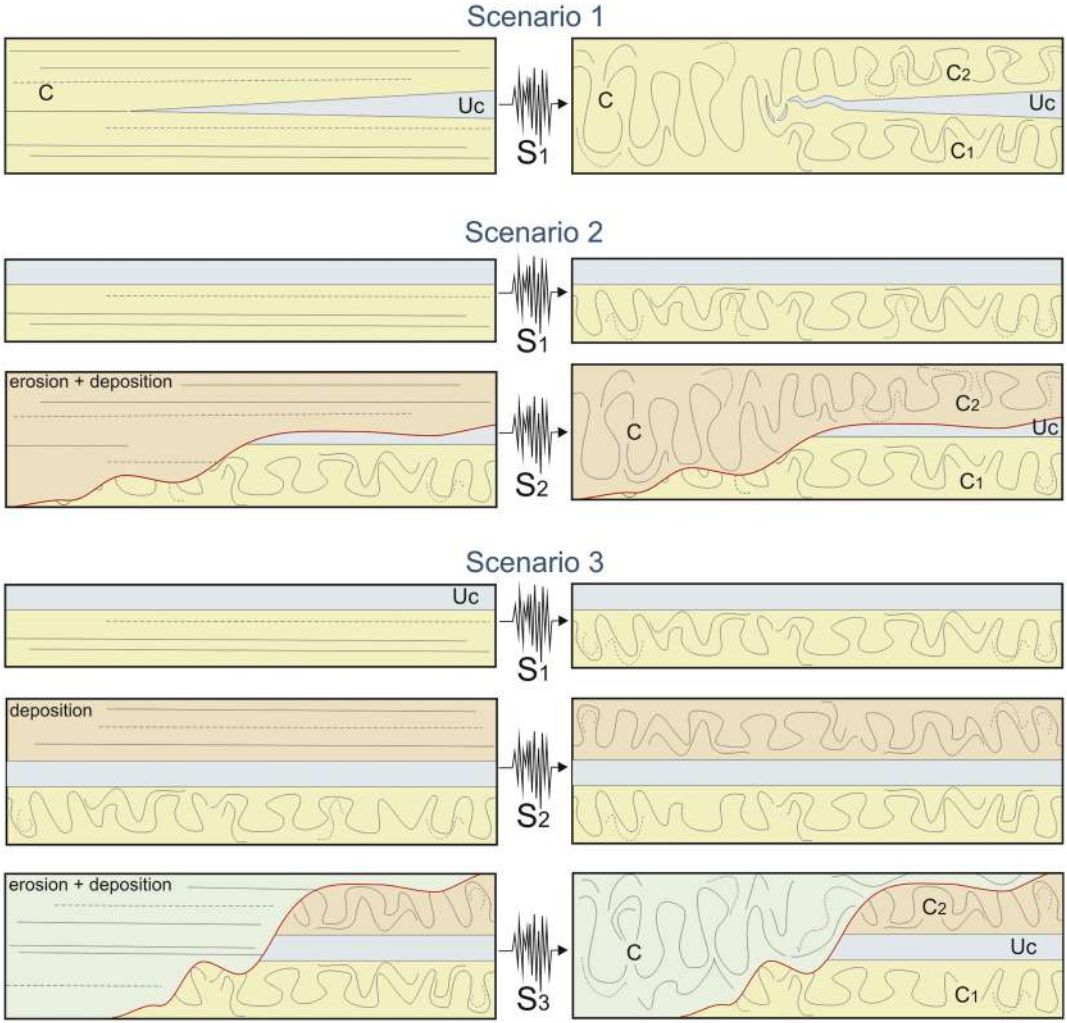
Scenario 1
C
Uc
S1
C
C2
Uc
C1
Scenario 2
S1
erosion + deposition
S2
C
C2
Uc
C1
Scenario 3
Uc
S1
deposition
S2
erosion + deposition
S3
C
C2
Uc
C1

Figure 11

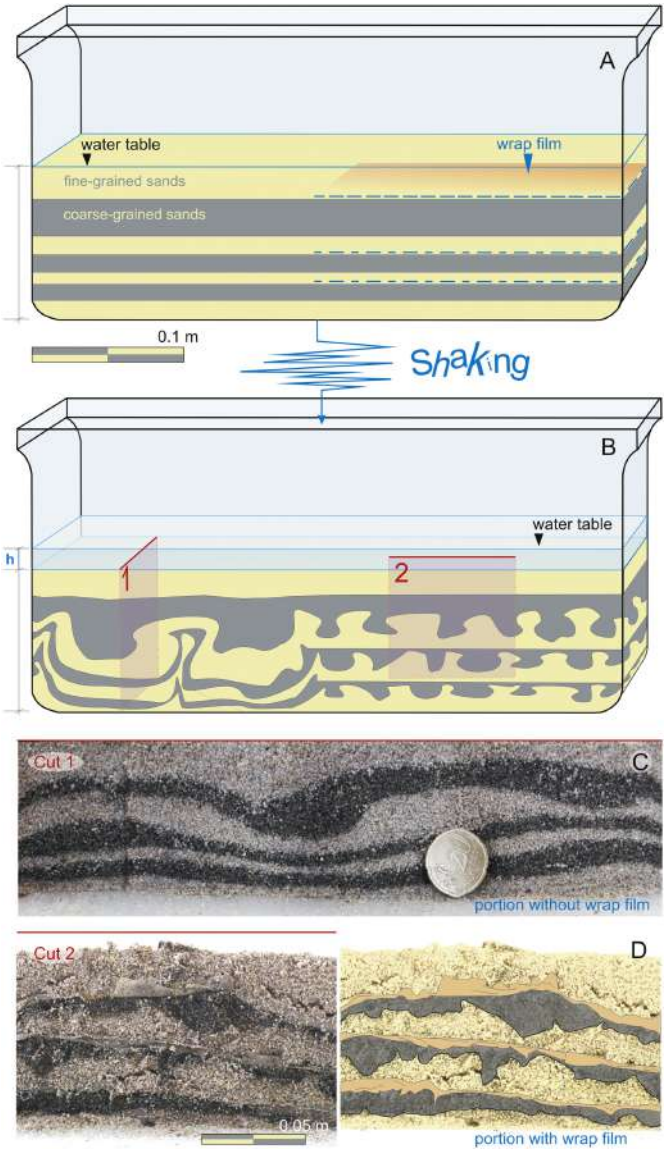
A
water table
wrap film
fine-grained sands
coarse-grained sands
0.1 m
Shaking
B
water table
h
1
2
Cut 1
C
portion without wrap film
Cut 2
0.05 m
D
portion with wrap film

Figure 12